Journal of Computational Physics 562 (2026) 115003

Contents lists available at ScienceDirect

Journal of Computational Physics

journal homepage: www.elsevier.com/locate/jcp

Novel linear, decoupled, and energy dissipative schemes for the Navier–Stokes–Darcy model and extension to related two-phase flow ⋆

Xiaoli Li [a], Jie Shen [b,*], Xinhui Wang [c]

[a] School of Mathematics and State Key Laboratory of Cryptography and Digital Economy Security, Shandong University, Jinan, Shandong, 250100, PR China
[b] School of Mathematical Science, Eastern Institute of Technology, Ningbo, China
[c] School of Mathematics, Shandong University, Jinan, Shandong, 250100, PR China

ARTICLE INFO

AMS subject classifications:
76D05
76T10
65M12

Keywords:
Navier–Stokes–Darcy model
Two-phase flows
Energy dissipation
Error estimates

ABSTRACT

We construct efficient original-energy-dissipative schemes for the Navier–Stokes–Darcy model and related two-phase flows using a prediction–correction framework. A new relaxation technique is incorporated in the correction step to guarantee dissipation of the original energy, thereby ensuring unconditional boundedness of the numerical solutions for the velocity and hydraulic head in the $l^\infty(L^2)$ and $l^2(H^1)$ norms. At each time step, the schemes require solving only a sequence of linear equations with constant coefficients. We rigorously prove that the schemes dissipate the original energy and, as an example, carry out a rigorous error analysis of the first-order scheme for the Navier–Stokes–Darcy model. Finally, a series of benchmark numerical experiments are conducted to demonstrate the accuracy, stability, and effectiveness of the proposed methods.

1. Introduction

The fluid-porous media system has broad applications across industrial processes and geophysical systems, attracting considerable research attention [1–6]. The coupled fluid-porous media system can be modeled mathematically by the incompressible Navier–Stokes equations for the free flow and Darcy's law for the flow in the porous media, coupled through interface conditions that enforce fundamental conservation laws: mass continuity and momentum balance, with tangential slip behavior described by the Beavers–Joseph–Saffman (BJS) condition [7,8].

Numerical simulation of free-flow–porous-media coupled systems has become a critical tool in subsurface engineering and environmental hydrology. Construction of structure-preserving schemes is crucial, as numerical solutions must faithfully approximate the exact solutions of the coupled model. Considerable research efforts have been devoted to developing numerical methods for the Navier–Stokes–Darcy model [8–17]. For instance, McCurdy et al. [2] conducted linear and nonlinear stability analyses of thermal convection in a fluid overlying a saturated porous medium, investigating the transition between full convection and fluid-dominated convection. They further developed a coarse-grained model and fully nonlinear schemes to predict convection patterns in coupled fluid-porous systems [18]. Rui and Zhang [19] designed a stabilized mixed finite element method for solving the coupled

⋆ This work is supported in part by the National Natural Science Foundation of China (Grant Nos.12271302, 12131014, W2431008 and 12371409) and Shandong Provincial Natural Science Foundation for Outstanding Youth Scholar (Grant No. ZR2024JQ030).

* Corresponding Author.
E-mail addresses: xiaolimath@sdu.edu.cn (X. Li), jshen@eitech.edu.cn (J. Shen), xinhuiwang0108@163.com (X. Wang).

https://doi.org/10.1016/j.jcp.2026.115003
Received 6 October 2025; Received in revised form 15 March 2026; Accepted 30 April 2026
Available online 6 May 2026

Stokes–Darcy system with solute transport. Chen et al. [17] proposed two second-order implicit–explicit schemes for the coupled Stokes–Darcy equations and established their unconditional stability. More recently, Chen et al. [20] introduced a family of fully decoupled numerical schemes for the extended Cahn–Hilliard–Navier–Stokes–Darcy–Boussinesq system, allowing the Navier–Stokes equations, Darcy equations, heat equation, and Cahn–Hilliard equation to be solved independently at each time step. In another direction, Qiu et al. [16] proposed a domain decomposition method for a time-dependent Navier–Stokes–Darcy model with Beavers–Joseph interface and defective boundary conditions, and rigorously established its convergence. Caucao et al. [21] proposed and analyzed a fully mixed finite element formulation for coupling free fluid flow with porous media flow. They also developed a reliable and efficient residual-based a posteriori error estimator for the proposed method. Hong et al. [22] proposed a numerical scheme for the non-stationary Stokes–Darcy model that significantly reduces computational costs compared to the standard finite element method.

As far as we know, all the aforementioned works rely on either an implicit or an implicit–explicit (IMEX) treatment of the nonlinear convection term in the Navier–Stokes equations, which leads to solving either a nonlinear system or a linear system with variable coefficients at each time step. From a computational perspective, it is highly desirable to treat the nonlinear term explicitly without imposing stability constraints. For instance, the IMEX schemes for the Navier–Stokes equations proposed in [23,24], based on the scalar auxiliary variable (SAV) approach [25,26], achieve unconditional energy stability while handling the nonlinear term explicitly. Improved variants can be found in [27,28]. Building on the ideas in [27], Jiang and Yang [29,30] developed efficient artificial compressibility ensemble schemes for Stokes–Darcy flow ensembles, while Wang et al. [31] constructed new IMEX schemes for the Navier–Stokes–Darcy model, combining the SAV approach in time with the finite element method in space. However, all these methods preserve only a modified energy, which differs from the model's original energy. Furthermore, the computational cost of solving the resulting linear systems [29,30] is typically about twice that of classical algorithms. Although there exists a class of Lagrange multiplier methods that can preserve the original energy dissipation [32], their implementation requires solving nonlinear algebraic systems. To the best of our knowledge, no existing work addresses the Navier–Stokes–Darcy model using a linear, decoupled, and explicit discretization of both the nonlinear convection and the coupled interface terms while still maintaining the original energy dissipation, let alone providing a convergence analysis.

Extending the methodology from the Navier–Stokes–Darcy model to the Cahn–Hilliard–Navier–Stokes–Darcy [33–38] system is crucial for accurately modeling multiphase flow dynamics in realistic applications. While the Navier–Stokes–Darcy model describes single-phase flow in coupled free flow and porous media regions, the Cahn–Hilliard–Navier–Stokes–Darcy model represents a natural extension to two-phase flow by incorporating the Cahn–Hilliard equation, which governs phase separation and interface evolution. This extension captures additional physical mechanisms, such as capillary forces and interfacial dynamics, that are essential for applications involving multiphase flow, including contaminant transport in groundwater and oil recovery processes. Although introducing the phase-field variable substantially increases the mathematical and computational complexity, it provides a more comprehensive and physically realistic framework. Developing energy-dissipative numerical schemes for this highly nonlinear multi-physics model not only addresses the challenges posed by the Cahn–Hilliard–Navier–Stokes–Darcy system, but also demonstrates the broader applicability and robustness of our proposed methodology.

The primary objective of this work is to construct linear, original-energy-dissipative schemes for the Navier–Stokes–Darcy model, and to extend them to two-phase flow problems. The main contributions of this paper are as follows:

- We develop first- and second-order linear prediction–correction schemes for the Navier–Stokes–Darcy model by proposing a new relaxation technique. These schemes are decoupled, requiring only the solution of a sequence of linear differential equations with constant coefficients at each time step. They preserve the model's original energy and consequently guarantee unconditional boundedness of the velocity and hydraulic head in the $l^\infty(L^2)$ and $l^2(H^1)$ norms.
- Both schemes are proved to be uniquely solvable and stable without any restriction on the time step. In addition, we establish optimal error estimates for the first-order scheme.
- We extend the proposed framework to the Cahn–Hilliard–Navier–Stokes–Darcy phase-field model. This extension retains key features of the original schemes, including linearity and preservation of the original energy.

The remainder of the paper is organized as follows. Section 2 formulates the Navier–Stokes–Darcy model and establishes its energy stability. In Section 3, we introduce first- and second-order linear, decoupled, and original-energy-dissipative schemes. Section 4 presents the theoretical analysis, proving unconditional energy stability, existence of solutions, and optimal convergence of velocity, hydraulic head, and energy via mathematical induction. Section 5 extends the methodology to the Cahn–Hilliard–Navier–Stokes–Darcy model with phase dynamics. Finally, Section 6 extends the three proposed numerical schemes to the EMAC formulation and presents numerical experiments, such as convergence tests, filtration processes, surface-tension relaxation tests and buoyancy-driven bubble dynamics. Some conclusions are given in the last section.

2. The Navier–Stokes–Darcy model

We start with some basic definitions. Consider a bounded domain $\Omega \subset \mathbb{R}^d$, $d = 2, 3$, which includes a free-flow domain Ω_f and a porous-media domain Ω_p. We denote the interface Γ between these two areas by $\Gamma = \partial\Omega_f \cap \partial\Omega_p$, and set $\Omega = \Omega_f \cup \Omega_p \cup \Gamma$. Here, the unit normal vector from Ω_f to Ω_p on Γ is defined as $\mathbf{n} = \mathbf{n}_f = -\mathbf{n}_p$. To simplify the notation, we further define $\Gamma_f = \partial\Omega_f \backslash \Gamma$, $\Gamma_p = \partial\Omega_p \backslash \Gamma$.

2.1. Model definition and concepts

In the free-flow domain Ω_f, the fluid satisfies the incompressible Navier–Stokes equations [39,40].

$$\partial_t \mathbf{u} - \nu\Delta\mathbf{u} + \nabla p + (\mathbf{u}\cdot\nabla)\mathbf{u} = \mathbf{f}_f, \quad \text{in } \Omega_f \times (0,T], \tag{2.1}$$
$$\nabla\cdot\mathbf{u} = 0, \quad \text{in } \Omega_f\times(0,T], \tag{2.2}$$
$$\mathbf{u}(\mathbf{x},0) = \mathbf{u}^0, \quad \text{in } \Omega_f, \tag{2.3}$$
$$\mathbf{u}(\mathbf{x},t) = \mathbf{0}, \quad \text{on } \Gamma_f\times(0,T]. \tag{2.4}$$

Here, the coefficient ν denotes the kinematic viscosity, which is inversely proportional to the Reynolds number Re. The final time is denoted by $T > 0$. $\mathbf{u}$ and p are the velocity and the pressure of free flow in Ω_f, respectively. $\mathbf{u}^0$ is the initial solution. The function $\mathbf{f}_f$ is an external body force.

In the porous-media domain Ω_p, the flow is governed by Darcy's law [41].

$$S_0\partial_t\phi - \nabla\cdot(\mathbb{K}\nabla\phi) = f_p, \quad \text{in } \Omega_p\times(0,T], \tag{2.5}$$
$$\phi(\mathbf{x},0) = \phi^0, \quad \text{in } \Omega_p, \tag{2.6}$$
$$\phi(\mathbf{x},t) = 0, \quad \text{on } \Gamma_p\times(0,T], \tag{2.7}$$

where ϕ is the hydraulic head in Ω_p, S_0 is a specific mass storage coefficient, f_p is the source/sink term, ϕ^0 is the initial solution, and the hydraulic conductivity tensor $\mathbb{K}$ is a symmetric positive-definite matrix.

On the interface Γ between the free-flow domain and the porous-media domain, we impose the following interface conditions:

$$\mathbf{u}\cdot\mathbf{n} + \mathbb{K}\nabla\phi\cdot\mathbf{n} = 0, \quad \text{on } \Gamma\times(0,T], \tag{2.8}$$
$$p - \nu\mathbf{n}\cdot(\nabla\mathbf{u}\cdot\mathbf{n}) + \frac{1}{2}|\mathbf{u}|^2 = g\phi, \text{on } \Gamma\times(0,T], \tag{2.9}$$
$$-\nu\boldsymbol{\tau}\cdot(\nabla\mathbf{u}\cdot\mathbf{n}) = \alpha\sqrt{\frac{\nu g}{tr(\mathbb{K})}}(\mathbf{u}\cdot\boldsymbol{\tau}), \text{on } \Gamma\times(0,T], \tag{2.10}$$

where g is the gravitational acceleration, $\boldsymbol{\tau}$ is the unit tangent vector, and α is a positive constant depending only on the structure of the porous medium. The first equation represents the continuity of the normal component of the velocity on the interface Γ, which means the conservation of mass. The second condition represents the balance of normal forces. In particular, we consider the inertial forces here, that is, the Lions interface condition [2,11,13,18]. The last equation is the Beavers–Joseph–Saffman interface condition [42,43].

We use $(\cdot,\cdot)_X$ (with $X = f$ or p) to denote the L^2 inner product in Ω_X, and $\|\cdot\|_X$ to denote the corresponding L^2 norm in Ω_X. In addition, we define

$$H_f = \{\mathbf{v}\in (H^1(\Omega_f))^d : \mathbf{v}|_{\Gamma_f} = 0\}, \qquad H_p = \{\psi\in H^1(\Omega_p) : \psi|_{\Gamma_p} = 0\},$$
$$Q_f = L^2(\Omega_f), \qquad W = H_f\times H_p.$$

Then, a weak formulation of the Navier–Stokes–Darcy model (2.1)–(2.10) is described as follows: $\forall\, t\in(0,T]$, find $\mathbf{u}\in H_f,\ p\in Q_f,\ \phi\in H_p$ such that

$$\begin{cases} (\partial_t\mathbf{u},\mathbf{v})_f + gS_0(\partial_t\phi,\psi)_p + \nu(\nabla\mathbf{u},\nabla\mathbf{v})_f - (p,\nabla\cdot\mathbf{v})_f + a(\mathbf{u},\mathbf{u},\mathbf{v}) + \alpha\sqrt{\frac{\nu g}{tr(\mathbb{K})}}\int_\Gamma(\mathbf{u}\cdot\boldsymbol{\tau})(\mathbf{v}\cdot\boldsymbol{\tau})ds \\ \quad + g(\mathbb{K}\nabla\phi,\nabla\psi)_p + c_\Gamma(\mathbf{v},\phi) - c_\Gamma(\mathbf{u},\psi) = (\mathbf{f}_f,\mathbf{v})_f + g(f_p,\psi)_p, \qquad \forall\mathbf{v}\in H_f,\ \psi\in H_p, \\ (\nabla\cdot\mathbf{u},q)_f = 0, \qquad \forall q\in Q_f, \\ (\mathbf{u}(\mathbf{x},0),\mathbf{v})_f = (\mathbf{u}^0,\mathbf{v})_f, \qquad \forall\mathbf{v}\in H_f, \\ (\phi(\mathbf{x},0),\psi)_p = (\phi^0,\psi)_p, \qquad \forall\psi\in H_p, \end{cases} \tag{2.11}$$

where

$$a(\mathbf{u},\mathbf{v},\mathbf{w}) = ((\mathbf{u}\cdot\nabla)\mathbf{v},\mathbf{w})_f - \frac{1}{2}\int_\Gamma(\mathbf{u}\cdot\mathbf{v})(\mathbf{w}\cdot\mathbf{n})ds, \qquad \forall\mathbf{u},\mathbf{v},\mathbf{w}\in H_f,$$
$$c_\Gamma(\mathbf{v},\phi) = g\int_\Gamma \phi\mathbf{v}\cdot\mathbf{n}ds, \qquad \forall\mathbf{v}\in H_f,\ \phi\in H_p.$$

Lemma 2.1. *Let $\mathbf{u}\in H_f$ and $\nabla\cdot\mathbf{u} = 0$, we have [31]*

$$a(\mathbf{u},\mathbf{v},\mathbf{v}) = 0, \quad \forall\mathbf{v}\in H_f. \tag{2.12}$$

Lemma 2.2. *For the nonlinear convective term $a(\mathbf{u},\mathbf{v},\mathbf{w})$, the following inequalities hold for $d=2,3$ [44,45]:*

$$a(\mathbf{u},\mathbf{v},\mathbf{w}) \le C\|\mathbf{u}\|_{1,f}\|\mathbf{v}\|_{1,f}\|\mathbf{w}\|_{1,f}, \tag{2.13}$$

$$a(\mathbf{u},\mathbf{v},\mathbf{w}) \le C\|\mathbf{u}\|_{0,f}\|\mathbf{v}\|_{2,f}\|\mathbf{w}\|_{1,f}, \tag{2.14}$$

$$a(\mathbf{u},\mathbf{v},\mathbf{w}) \le C\|\mathbf{u}\|_{2,f}\|\mathbf{v}\|_{0,f}\|\mathbf{w}\|_{1,f}; \tag{2.15}$$

and when $d=2$, we have

$$\left|\int_\Gamma (\mathbf{u}\cdot\mathbf{v})(\mathbf{w}\cdot\boldsymbol{n})ds\right| \le C\|\mathbf{u}\|_{0,f}^{1/2}\|\mathbf{u}\|_{1,f}^{1/2}\|\mathbf{v}\|_{0,f}^{1/2}\|\mathbf{v}\|_{1,f}^{1/2}\|\mathbf{w}\|_{0,f}^{1/2}\|\mathbf{w}\|_{1,f}^{1/2}, \tag{2.16}$$

$$a(\mathbf{u},\mathbf{v},\mathbf{w}) \le C\|\mathbf{u}\|_{0,f}^{1/2}\|\mathbf{u}\|_{1,f}^{1/2}\|\mathbf{v}\|_{0,f}^{1/2}\|\mathbf{v}\|_{1,f}^{1/2}\|\mathbf{w}\|_{1,f}, \tag{2.17}$$

where C is a positive constant.

2.2. Energy dissipation law

We show below that the problem (2.11) is energy dissipative if $\mathbf{f}_f=\mathbf{0}$ and $f_p=0$. Indeed, substituting $\mathbf{v}=\mathbf{u}$ and $\psi=\phi$ into (2.11), we obtain

$$\begin{aligned}&(\partial_t\mathbf{u},\mathbf{u})_f + gS_0(\partial_t\phi,\phi)_p + \nu(\nabla\mathbf{u},\nabla\mathbf{u})_f + a(\mathbf{u},\mathbf{u},\mathbf{u}) + \alpha\sqrt{\frac{\nu g}{tr(\mathbb{K})}}\int_\Gamma(\mathbf{u}\cdot\boldsymbol{\tau})^2 ds\\ &\quad + g(\mathbb{K}\nabla\phi,\nabla\phi)_p + c_\Gamma(\mathbf{u},\phi) - c_\Gamma(\mathbf{u},\phi) = 0, \qquad \forall \mathbf{v}\in H_f,\ \psi\in H_p.\end{aligned}$$

Thanks to (2.12), we derive from the above that

$$\frac{1}{2}\frac{d}{dt}\|\mathbf{u}\|_f^2 + \frac{gS_0}{2}\frac{d}{dt}\|\phi\|_p^2 = -\nu(\nabla\mathbf{u},\nabla\mathbf{u})_f - \alpha\sqrt{\frac{\nu g}{tr(\mathbb{K})}}\int_\Gamma(\mathbf{u}\cdot\boldsymbol{\tau})^2ds - g(\mathbb{K}\nabla\phi,\nabla\phi)_p \le 0. \tag{2.18}$$

In other words, we have

$$\frac{dE}{dt}\le 0, \quad \text{where } E = \frac{1}{2}\|\mathbf{u}\|_f^2 + \frac{gS_0}{2}\|\phi\|_p^2.$$

3. Energy stable schemes

In order to construct efficient and unconditionally energy stable schemes, we introduce a scalar auxiliary variable $\xi(t)\equiv 1$, which serves as a relaxation factor, and expand the original system (2.11) with a reformulated energy dissipation law:

$$\frac{1}{2}\frac{d}{dt}\|\mathbf{u}\|_f^2 + \frac{gS_0}{2}\frac{d}{dt}\|\phi\|_p^2 = \xi(t)\Big(-\nu(\nabla\mathbf{u},\nabla\mathbf{u})_f - \alpha\sqrt{\frac{\nu g}{tr(\mathbb{K})}}\int_\Gamma(\mathbf{u}\cdot\boldsymbol{\tau})^2ds - g(\mathbb{K}\nabla\phi,\nabla\phi)_p\Big). \tag{3.1}$$

3.1. Scheme I: a first-order scheme

We now construct a first-order scheme for the expanded system, i.e., (2.11) and (3.1), using a prediction–correction approach as follows: We begin by introducing a uniform partition of the interval $[0,T]$ with grid points $0=t_0<t_1<\cdots<t_M=T$ and a constant time step size $\Delta t = t_{n+1}-t_n = T/M$.

Step 1 (Prediction). Given $(\mathbf{u}^n,p^n,\phi^n)$ and $(\tilde{\mathbf{u}}^n,\tilde\phi^n)$, for any $(\mathbf{v},q,\psi)\in H_f\times Q_f\times H_p$, find $(\tilde{\mathbf{u}}^{n+1},p^{n+1},\tilde\phi^{n+1})$ satisfying

$$\begin{aligned}&\left(\frac{\tilde{\mathbf{u}}^{n+1}-\tilde{\mathbf{u}}^n}{\Delta t},\mathbf{v}\right)_f + \nu(\nabla\tilde{\mathbf{u}}^{n+1},\nabla\mathbf{v})_f + \alpha\sqrt{\frac{\nu g}{tr(\mathbb{K})}}\int_\Gamma(\tilde{\mathbf{u}}^{n+1}\cdot\boldsymbol{\tau})(\mathbf{v}\cdot\boldsymbol{\tau})ds - (p^{n+1},\nabla\cdot\mathbf{v})_f\\ &+ a(\mathbf{u}^n,\mathbf{u}^n,\mathbf{v}) + c_\Gamma(\mathbf{v},\phi^n) = (\mathbf{f}_f^{n+1},\mathbf{v})_f,\end{aligned} \tag{3.2}$$

$$(\nabla\cdot\tilde{\mathbf{u}}^{n+1},q)_f = 0, \tag{3.3}$$

$$gS_0\left(\frac{\tilde\phi^{n+1}-\tilde\phi^n}{\Delta t},\psi\right)_p + g(\mathbb{K}\nabla\tilde\phi^{n+1},\nabla\psi)_p - c_\Gamma(\mathbf{u}^n,\psi) = g(f_p^{n+1},\psi)_p. \tag{3.4}$$

Step 2 (Correction). We denote

$$\tilde E^{n+1} = \frac{1}{2}\|\tilde{\mathbf{u}}^{n+1}\|_f^2 + \frac{gS_0}{2}\|\tilde\phi^{n+1}\|_p^2, \tag{3.5}$$

and set

$$E^{n+1} = \xi^{n+1}\tilde E^{n+1}, \tag{3.6}$$

where ξ^{n+1}, which is an approximation of 1, satisfies the linear algebraic equation

$$\frac{E^{n+1}-E^n}{\Delta t} = -\xi^{n+1}\left(\nu\|\nabla\tilde{\mathbf{u}}^{n+1}\|_f^2 + \alpha\sqrt{\frac{\nu g}{tr(\mathbb{K})}}\int_\Gamma(\tilde{\mathbf{u}}^{n+1}\cdot\boldsymbol{\tau})^2ds + g\|\sqrt{\mathbb{K}}\nabla\tilde\phi^{n+1}\|_p^2\right). \tag{3.7}$$

Finally, we update $\mathbf{u}^{n+1}$ and ϕ^{n+1} by

$$\mathbf{u}^{n+1} = \sqrt{\xi^{n+1}}\tilde{\mathbf{u}}^{n+1}, \qquad \phi^{n+1} = \sqrt{\xi^{n+1}}\tilde\phi^{n+1}. \tag{3.8}$$

Theorem 3.1. *If $E^n \geq 0$, we have $\xi^{n+1} \geq 0$, $E^{n+1} \geq 0$. Hence, the scheme (3.2)–(3.8) dissipates the original energy as shown by (3.7). Moreover, we have*

$$\frac{1}{2}\|\mathbf{u}^{k+1}\|_f^2 + \frac{gS_0}{2}\|\phi^{k+1}\|_p^2 + \Delta t \sum_{n=0}^{k} \left(\nu\|\nabla \mathbf{u}^{n+1}\|_f^2 + \alpha\sqrt{\frac{\nu g}{tr(\mathbb{K})}} \int_\Gamma (\mathbf{u}^{n+1}\cdot\boldsymbol{\tau})^2 ds + g\|\sqrt{\mathbb{K}}\nabla\phi^{n+1}\|_p^2 \right)$$
$$= \frac{1}{2}\|\mathbf{u}^0\|_f^2 + \frac{gS_0}{2}\|\phi^0\|_p^2 \leq C, \tag{3.9}$$

where C is a positive constant that depends on the initial conditions ϕ^0 and $\mathbf{u}^0$.

Proof. Since $E^n \geq 0$, $\tilde{E}^{n+1} \geq 0$ and $E^{n+1} = \xi^{n+1}\tilde{E}^{n+1}$, one derives immediately from (3.7) that

$$\xi^{n+1} = \frac{E^n}{\tilde{E}^{n+1} + \Delta t \mathbb{A}(\tilde{\mathbf{u}}^{n+1}, \tilde{\phi}^{n+1})} \geq 0, \tag{3.10}$$

where $\mathbb{A}(\tilde{\mathbf{u}}^{n+1}, \tilde{\phi}^{n+1}) = \nu\|\nabla\tilde{\mathbf{u}}^{n+1}\|_f^2 + \alpha\sqrt{\frac{\nu g}{tr(\mathbb{K})}}\int_\Gamma (\tilde{\mathbf{u}}^{n+1}\cdot\boldsymbol{\tau})^2 ds + g\|\sqrt{\mathbb{K}}\nabla\tilde{\phi}^{n+1}\|_p^2 \geq 0$.

Combining (3.7) and (3.10), we find

$$\frac{E^{n+1} - E^n}{\Delta t} = -\xi^{n+1}\mathbb{A}(\tilde{\mathbf{u}}^{n+1}, \tilde{\phi}^{n+1}) \leq 0, \tag{3.11}$$

which indicates that the original energy is dissipative.

On the other hand, summing up (3.7) from $n = 0$ to $n = k$, we obtain

$$E^{k+1} + \Delta t \sum_{n=0}^{k} \xi^{n+1}\mathbb{A}(\tilde{\mathbf{u}}^{n+1}, \tilde{\phi}^{n+1}) = E^0 \leq C,$$

which implies (3.9). □

3.2. *Scheme II: a second-order scheme*

Similarly, we can construct a second-order scheme based on the Crank-Nicolson and Adam-Bashforth formula as follows:

Step 1 (Prediction). Given $(\mathbf{u}^{n-1}, \phi^{n-1})$, $(\mathbf{u}^n, p^n, \phi^n)$ and $(\tilde{\mathbf{u}}^n, \tilde{\phi}^n)$, for any $(\mathbf{v}, q, \psi) \in H_f \times Q_f \times H_p$, find $(\tilde{\mathbf{u}}^{n+1}, p^{n+1}, \tilde{\phi}^{n+1})$ satisfying

$$\left(\frac{\tilde{\mathbf{u}}^{n+1} - \tilde{\mathbf{u}}^n}{\Delta t}, \mathbf{v}\right)_f + \nu\left(\nabla\left(\frac{\tilde{\mathbf{u}}^{n+1} + \mathbf{u}^n}{2}\right), \nabla\mathbf{v}\right)_f + \alpha\sqrt{\frac{\nu g}{tr(\mathbb{K})}}\int_\Gamma\left(\frac{\tilde{\mathbf{u}}^{n+1} + \mathbf{u}^n}{2}\cdot\boldsymbol{\tau}\right)(\mathbf{v}\cdot\boldsymbol{\tau})ds$$
$$-\left(\frac{p^{n+1} + p^n}{2}, \nabla\cdot\mathbf{v}\right)_f + a(\tilde{\mathbf{u}}^{n+\frac{1}{2}}, \tilde{\mathbf{u}}^{n+\frac{1}{2}}, \mathbf{v}) + c_\Gamma(\mathbf{v}, \tilde{\phi}^{n+\frac{1}{2}}) = \left(\frac{\mathbf{f}_f^{n+1} + \mathbf{f}_f^n}{2}, \mathbf{v}\right)_f, \tag{3.12}$$

$$(\nabla\cdot\tilde{\mathbf{u}}^{n+1}, q)_f = 0, \tag{3.13}$$

$$gS_0\left(\frac{\tilde{\phi}^{n+1} - \tilde{\phi}^n}{\Delta t}, \psi\right)_p + g\left(\mathbb{K}\nabla\frac{\tilde{\phi}^{n+1} + \phi^n}{2}, \nabla\psi\right)_p - c_\Gamma(\tilde{\mathbf{u}}^{n+\frac{1}{2}}, \psi) = g\left(\frac{f_p^{n+1} + f_p^n}{2}, \psi\right)_p, \tag{3.14}$$

where $\tilde{\mathbf{u}}^{n+\frac{1}{2}} = \frac{3}{2}\mathbf{u}^n - \frac{1}{2}\mathbf{u}^{n-1}$ and $\tilde{\phi}^{n+\frac{1}{2}} = \frac{3}{2}\phi^n - \frac{1}{2}\phi^{n-1}$.

Step 2 (Correction). We denote

$$\tilde{E}^{n+1} = \frac{1}{2}\|\tilde{\mathbf{u}}^{n+1}\|_f^2 + \frac{gS_0}{2}\|\tilde{\phi}^{n+1}\|_p^2, \tag{3.15}$$

and set

$$E^{n+1} = \xi^{n+1}\tilde{E}^{n+1}, \tag{3.16}$$

where ξ^{n+1}, which is an approximation of 1, satisfies the linear algebraic equation

$$\frac{E^{n+1} - E^n}{\Delta t} = -\xi^{n+1}\left(\nu\left\|\nabla\left(\frac{\tilde{\mathbf{u}}^{n+1} + \mathbf{u}^n}{2}\right)\right\|_f^2 + \alpha\sqrt{\frac{\nu g}{tr(\mathbb{K})}}\int_\Gamma\left(\frac{\tilde{\mathbf{u}}^{n+1} + \mathbf{u}^n}{2}\cdot\boldsymbol{\tau}\right)^2 ds\right.$$
$$\left. + g\left\|\sqrt{\mathbb{K}}\nabla\frac{\tilde{\phi}^{n+1} + \phi^n}{2}\right\|_p^2\right). \tag{3.17}$$

Finally, we update $\mathbf{u}^{n+1}$ and ϕ^{n+1} by

$$\mathbf{u}^{n+1} = \sqrt{\xi^{n+1}}\tilde{\mathbf{u}}^{n+1}, \qquad \phi^{n+1} = \sqrt{\xi^{n+1}}\tilde{\phi}^{n+1}. \tag{3.18}$$

Similarly as in the proof of Theorem 3.1, we can establish the following result:

Theorem 3.2. *If $E^n \geq 0$, we have $\xi^{n+1} \geq 0$, $E^{n+1} \geq 0$. Hence, the scheme (3.12)–(3.18) dissipates the original energy as shown by (3.17).*

4. Error analysis

The primary goal of this section is to carry out an error analysis for **Scheme I** (3.2)–(3.8). Hereafter, we use C to denote the general positive constant, independent of Δt, whose value may differ in different contexts. For the sake of simplicity, we assume that the hydraulic conductivity tensor $\mathbb{K} = K\mathbb{J}$ during the theoretical analysis, where $K > 0$ is a scalar coefficient and $\mathbb{J}$ denotes the identity tensor.

Assume that the exact solution and initial data of the problem (2.11) satisfy the following regularity properties:

$$\begin{cases} \mathbf{u} \in L^\infty(0,T;H^2(\Omega_f)), \quad \partial_t \mathbf{u} \in L^2(0,T;H^2(\Omega_f)), \quad \partial_{tt}\mathbf{u} \in L^2(0,T;H^{-1}(\Omega_f)),\\ p \in L^2(0,T;H^1(\Omega_f)),\\ \phi \in L^\infty(0,T;H^2(\Omega_p)), \quad \partial_t\phi \in L^2(0,T;H^2(\Omega_p)), \quad \partial_{tt}\phi \in L^2(0,T;H^{-1}(\Omega_p)),\\ \mathbf{u}(t^0) \in L^2(\Omega_f), \quad \phi(t^0) \in L^2(\Omega_p), \quad \mathbf{f}_f \in L^2(0,T;H^{-1}(\Omega_f)), \quad f_p \in L^2(0,T;H^{-1}(\Omega_p)). \end{cases} \tag{4.1}$$

For the subsequent error analysis, we restrict our attention to the two-dimensional case. The extension to three-dimension is more challenging and will be addressed in future work.

4.1. A rough error estimate

The errors between the numerical and exact solutions are defined as follows:

$$e_E^{n+1} = E^{n+1} - E(t^{n+1}), \quad e_{\mathbf{u}}^{n+1} = \mathbf{u}^{n+1} - \mathbf{u}(t^{n+1}), \quad e_\phi^{n+1} = \phi^{n+1} - \phi(t^{n+1}),$$
$$\tilde{e}_E^{n+1} = \tilde{E}^{n+1} - E(t^{n+1}), \quad \tilde{e}_{\mathbf{u}}^{n+1} = \tilde{\mathbf{u}}^{n+1} - \mathbf{u}(t^{n+1}), \quad \tilde{e}_\phi^{n+1} = \tilde{\phi}^{n+1} - \phi(t^{n+1}).$$

We set $\tilde{\mathbf{u}}^0 = \mathbf{u}(t^0)$ and $\tilde{\phi}^0 = \phi(t^0)$, so it is easy to see that

$$\|\tilde{e}_{\mathbf{u}}^0\|_f + \|\tilde{e}_\phi^0\|_p = 0, \quad |e_E^0| = 0.$$

Lemma 4.1. *Given $1 \le k \le T/\Delta t - 1$, we assume that the following error estimates hold*

$$\|\tilde{e}_{\mathbf{u}}^m\|_f + \|\tilde{e}_\phi^m\|_p \le \hat{C}\Delta t^{\frac{1}{4}}, \quad m = 1, \dots, k, \tag{4.2}$$
$$|e_E^m| \le C^*\Delta t^{1-\gamma}, \quad \gamma > 0, \quad m = 1, \dots, k, \tag{4.3}$$

where $\hat{C}$ and C^* are two fixed positive constants independent of Δt. Then, under the regularity assumption (4.1), and for Δt sufficiently small, we have

$$\|\tilde{e}_{\mathbf{u}}^{k+1}\|_f + \|\tilde{e}_\phi^{k+1}\|_p \le \hat{C}\Delta t^{\frac{1}{4}}, \tag{4.4}$$

where $\hat{C}$ is the positive constant in (4.2).

Proof. Let $1 \le n \le k$. Based on assumptions (4.2)–(4.3), we can derive

$$0 < \frac{1}{2}E(t^n) \le \tilde{E}^n \le \frac{3}{2}E(t^n). \tag{4.5}$$

Also, from Theorem 3.1 and the regularity properties (4.1), we have

$$\xi^n = \frac{E^n}{\tilde{E}^n} \le \frac{2E^n}{E(t^n)} \le C_1^2, \tag{4.6}$$

where C_1 is a fixed positive constant independent of Δt. We derive from (2.11) that

$$\begin{aligned} &\left(\frac{\mathbf{u}(t^{n+1}) - \mathbf{u}(t^n)}{\Delta t}, \mathbf{v}\right)_f + \nu(\nabla\mathbf{u}(t^{n+1}), \nabla\mathbf{v})_f + \alpha\sqrt{\frac{\nu g}{tr(\mathbb{K})}}\int_\Gamma (\mathbf{u}(t^{n+1})\cdot\boldsymbol{\tau})(\mathbf{v}\cdot\boldsymbol{\tau})ds\\ &- (p(t^{n+1}), \nabla\cdot\mathbf{v})_f + a(\mathbf{u}(t^{n+1}), \mathbf{u}(t^{n+1}), \mathbf{v}) + c_\Gamma(\mathbf{v}, \phi(t^{n+1}))\\ &= (\mathbf{f}_f^{n+1}, \mathbf{v})_f + R_u^{n+1}(\mathbf{v}), \end{aligned} \tag{4.7}$$

where $R_u^{n+1}(\mathbf{v}) = \left(\frac{\mathbf{u}(t^{n+1})-\mathbf{u}(t^n)}{\Delta t} - \frac{\partial\mathbf{u}(t^{n+1})}{\partial t}, \mathbf{v}\right)_f$. Subtracting (4.7) from (3.2), we obtain

$$\begin{aligned} &\left(\frac{\tilde{e}_{\mathbf{u}}^{n+1} - \tilde{e}_{\mathbf{u}}^n}{\Delta t}, \mathbf{v}\right)_f + \nu(\nabla\tilde{e}_{\mathbf{u}}^{n+1}, \nabla\mathbf{v})_f + \alpha\sqrt{\frac{\nu g}{tr(\mathbb{K})}}\int_\Gamma (\tilde{e}_{\mathbf{u}}^{n+1}\cdot\boldsymbol{\tau})(\mathbf{v}\cdot\boldsymbol{\tau})ds\\ &- (p^{n+1} - p(t^{n+1}), \nabla\cdot\mathbf{v})_f + a(\mathbf{u}^n, \mathbf{u}^n, \mathbf{v}) - a(\mathbf{u}(t^{n+1}), \mathbf{u}(t^{n+1}), \mathbf{v})\\ &+ c_\Gamma(\mathbf{v}, \phi^n) - c_\Gamma(\mathbf{v}, \phi(t^{n+1})) = -R_{\mathbf{u}}^{n+1}(\mathbf{v}). \end{aligned}$$

Taking $\mathbf{v} = \tilde{e}_{\mathbf{u}}^{n+1}$ in the above equation, we get

$$\begin{aligned}
&\frac{1}{2\Delta t}\Big(\|\tilde{e}_{\mathbf{u}}^{n+1}\|_f^2 - \|\tilde{e}_{\mathbf{u}}^{n}\|_f^2 + \|\tilde{e}_{\mathbf{u}}^{n+1} - \tilde{e}_{\mathbf{u}}^{n}\|_f^2\Big) + \nu\|\nabla\tilde{e}_{\mathbf{u}}^{n+1}\|_f^2 + \alpha\sqrt{\frac{\nu g}{tr(\mathbb{K})}}\int_\Gamma (\tilde{e}_{\mathbf{u}}^{n+1}\cdot\boldsymbol{\tau})^2 ds \\
&= -R_{\mathbf{u}}^{n+1}(\tilde{e}_{\mathbf{u}}^{n+1}) - a(\mathbf{u}^n, \mathbf{u}^n, \tilde{e}_{\mathbf{u}}^{n+1}) + a(\mathbf{u}(t^{n+1}), \mathbf{u}(t^{n+1}), \tilde{e}_{\mathbf{u}}^{n+1}) - c_\Gamma(\tilde{e}_{\mathbf{u}}^{n+1}, \phi^n) + c_\Gamma(\tilde{e}_{\mathbf{u}}^{n+1}, \phi(t^{n+1})) \\
&= \sum_{i=1}^{3} I_i.
\end{aligned} \tag{4.8}$$

Now, we aim to estimate the right-hand side terms of (4.8) successively. Based on Lemma 2.2, Cauchy-Schwarz and Young's inequalities, we get

$$|I_1| = |-R_{\mathbf{u}}^{n+1}(\tilde{e}_{\mathbf{u}}^{n+1})| \le \epsilon_{\mathbf{u}}\nu\|\nabla\tilde{e}_{\mathbf{u}}^{n+1}\|_f^2 + C\Delta t\int_{t^n}^{t^{n+1}} \|\partial_{tt}\mathbf{u}\|_{-1,f}^2 dt,$$

$$\begin{aligned}
|I_2| &= |-a(\mathbf{u}^n, \mathbf{u}^n, \tilde{e}_{\mathbf{u}}^{n+1}) + a(\mathbf{u}(t^{n+1}), \mathbf{u}(t^{n+1}), \tilde{e}_{\mathbf{u}}^{n+1})| \\
&= |a(\mathbf{u}(t^{n+1}) - \mathbf{u}(t^n), \mathbf{u}(t^{n+1}), \tilde{e}_{\mathbf{u}}^{n+1}) - a(e_{\mathbf{u}}^n, \mathbf{u}(t^{n+1}), \tilde{e}_{\mathbf{u}}^{n+1}) + a(\mathbf{u}^n, \mathbf{u}(t^{n+1}) - \mathbf{u}(t^n), \tilde{e}_{\mathbf{u}}^{n+1}) \\
&\quad - a(e_{\mathbf{u}}^n, e_{\mathbf{u}}^n, \tilde{e}_{\mathbf{u}}^{n+1}) - a(\mathbf{u}(t^n), e_{\mathbf{u}}^n, \tilde{e}_{\mathbf{u}}^{n+1})| \\
&\le C\|\mathbf{u}(t^{n+1}) - \mathbf{u}(t^n)\|_f\|\mathbf{u}(t^{n+1})\|_{2,f}\|\nabla\tilde{e}_{\mathbf{u}}^{n+1}\|_f + C\|e_{\mathbf{u}}^n\|_f\|\mathbf{u}(t^{n+1})\|_{2,f}\|\nabla\tilde{e}_{\mathbf{u}}^{n+1}\|_f \\
&\quad + C\|\mathbf{u}^n\|_f\|\mathbf{u}(t^{n+1}) - \mathbf{u}(t^n)\|_{2,f}\|\nabla\tilde{e}_{\mathbf{u}}^{n+1}\|_f + C\|e_{\mathbf{u}}^n\|_f^{1/2}\|\nabla e_{\mathbf{u}}^n\|_f^{1/2}\|e_{\mathbf{u}}^n\|_f^{1/2}\|\nabla e_{\mathbf{u}}^n\|_f^{1/2}\|\nabla\tilde{e}_{\mathbf{u}}^{n+1}\|_f \\
&\quad + C\|\mathbf{u}(t^n)\|_{2,f}\|e_{\mathbf{u}}^n\|_f\|\nabla\tilde{e}_{\mathbf{u}}^{n+1}\|_f \\
&\le \epsilon_{\mathbf{u}}\nu\|\nabla\tilde{e}_{\mathbf{u}}^{n+1}\|_f^2 + C\|e_{\mathbf{u}}^n\|_f^2 + C\|\nabla e_{\mathbf{u}}^n\|_f^2\|e_{\mathbf{u}}^n\|_f^2 + C\Delta t\int_{t^n}^{t^{n+1}} \|\partial_t\mathbf{u}\|_f^2 dt + C\Delta t\int_{t^n}^{t^{n+1}} \|\partial_t\mathbf{u}\|_{2,f}^2 dt,
\end{aligned}$$

$$\begin{aligned}
|I_3| &= |-c_\Gamma(\tilde{e}_{\mathbf{u}}^{n+1}, \phi^n) + c_\Gamma(\tilde{e}_{\mathbf{u}}^{n+1}, \phi(t^{n+1}))| \\
&\le |c_\Gamma(\tilde{e}_{\mathbf{u}}^{n+1}, \phi(t^{n+1}) - \phi(t^n))| + |c_\Gamma(\tilde{e}_{\mathbf{u}}^{n+1}, e_\phi^n)| \\
&\le \epsilon_{\mathbf{u}}\nu\|\nabla\tilde{e}_{\mathbf{u}}^{n+1}\|_f^2 + C\|e_\phi^n\|_p\|\nabla e_\phi^n\|_p + C\Delta t\int_{t^n}^{t^{n+1}} \|\partial_t\phi\|_{1,p}^2 dt.
\end{aligned}$$

We notice that there are some remaining terms that still need to be analyzed. Based on the regularity properties (4.1) and the boundedness of $\tilde{E}^n$ and ξ^n in (4.5)-(4.6), we have

$$\begin{aligned}
\|e_{\mathbf{u}}^n\|_f = \|\sqrt{\xi^n}\tilde{\mathbf{u}}^n - \mathbf{u}(t^n)\|_f &\le \|\sqrt{\xi^n}(\tilde{\mathbf{u}}^n - \mathbf{u}(t^n))\|_f + \|(\sqrt{\xi^n} - 1)\mathbf{u}(t^n)\|_f \\
&\le C_1\|\tilde{e}_{\mathbf{u}}^n\|_f + C\left|\frac{\xi^n - 1}{\sqrt{\xi^n} + 1}\right| \\
&\le C_1\|\tilde{e}_{\mathbf{u}}^n\|_f + C\left|\frac{E^n - E(t^n)}{\tilde{E}^n}\right| + C\left|\frac{E(t^n) - \tilde{E}^n}{\tilde{E}^n}\right| \\
&\le C\|\tilde{e}_{\mathbf{u}}^n\|_f + C\|\tilde{e}_\phi^n\|_p + C|e_E^n|.
\end{aligned} \tag{4.9}$$

Similarly, we can also obtain that

$$\|e_\phi^n\|_p \le C\|\tilde{e}_{\mathbf{u}}^n\|_f + C\|\tilde{e}_\phi^n\|_p + C|e_E^n|, \tag{4.10}$$

$$\|\nabla e_{\mathbf{u}}^n\|_f \le C_1\|\nabla\tilde{e}_{\mathbf{u}}^n\|_f + C\|\tilde{e}_{\mathbf{u}}^n\|_f + C\|\tilde{e}_\phi^n\|_p + C|e_E^n|, \tag{4.11}$$

$$\|\nabla e_\phi^n\|_p \le C_1\|\nabla\tilde{e}_\phi^n\|_p + C\|\tilde{e}_{\mathbf{u}}^n\|_f + C\|\tilde{e}_\phi^n\|_p + C|e_E^n|. \tag{4.12}$$

Then we get

$$\begin{aligned}
&\frac{1}{2\Delta t}\Big(\|\tilde{e}_{\mathbf{u}}^{n+1}\|_f^2 - \|\tilde{e}_{\mathbf{u}}^{n}\|_f^2 + \|\tilde{e}_{\mathbf{u}}^{n+1} - \tilde{e}_{\mathbf{u}}^{n}\|_f^2\Big) + \nu\|\nabla\tilde{e}_{\mathbf{u}}^{n+1}\|_f^2 + \alpha\sqrt{\frac{\nu g}{tr(\mathbb{K})}}\int_\Gamma (\tilde{e}_{\mathbf{u}}^{n+1}\cdot\boldsymbol{\tau})^2 ds \\
&\le 3\epsilon_{\mathbf{u}}\nu\|\nabla\tilde{e}_{\mathbf{u}}^{n+1}\|_f^2 + \epsilon_\phi gK\|\nabla\tilde{e}_\phi^n\|_p^2 + C\|\tilde{e}_{\mathbf{u}}^n\|_f^2 + C|e_E^n|^2 + C\|\tilde{e}_\phi^n\|_p^2 + C\|\nabla e_{\mathbf{u}}^n\|_f^2\|\tilde{e}_{\mathbf{u}}^n\|_f^2 \\
&\quad + C\|\nabla e_{\mathbf{u}}^n\|_f^2\|\tilde{e}_\phi^n\|_p^2 + C\|\nabla e_{\mathbf{u}}^n\|_f^2|e_E^n|^2 + C\Delta t\int_{t^n}^{t^{n+1}} \|\partial_{tt}\mathbf{u}\|_{-1,f}^2 dt + C\Delta t\int_{t^n}^{t^{n+1}} \|\partial_t\mathbf{u}\|_f^2 dt \\
&\quad + C\Delta t\int_{t^n}^{t^{n+1}} \|\partial_t\mathbf{u}\|_{2,f}^2 dt + C\Delta t\int_{t^n}^{t^{n+1}} \|\partial_t\phi\|_{1,p}^2 dt.
\end{aligned} \tag{4.13}$$

Now, we focus on the error estimate of the hydraulic head. Consider the equation satisfied by the exact solution $\phi(t^{n+1})$.

$$gS_0\left(\frac{\phi(t^{n+1}) - \phi(t^n)}{\Delta t}, \psi\right)_p + g(\mathbb{K}\nabla\phi(t^{n+1}), \nabla\psi)_p - c_\Gamma(\mathbf{u}(t^{n+1}), \psi) = g(f_p^{n+1}, \psi)_p + R_\phi^{n+1}(\psi), \tag{4.14}$$

where $R_{\phi}^{n+1}(\psi) = gS_0\left(\frac{\phi(t^{n+1})-\phi(t^n)}{\Delta t} - \frac{\partial\phi(t^{n+1})}{\partial t}, \psi\right)_p$. Subtracting (4.14) from (3.4), we obtain

$$gS_0\left(\frac{\tilde{e}_{\phi}^{n+1}-\tilde{e}_{\phi}^{n}}{\Delta t}, \psi\right)_p + g(\mathbb{K}\nabla\tilde{e}_{\phi}^{n+1}, \nabla\psi)_p - c_{\Gamma}(\mathbf{u}^n, \psi) + c_{\Gamma}(\mathbf{u}(t^{n+1}), \psi) = -R_{\phi}^{n+1}(\psi).$$

Substituting $\psi = \tilde{e}_{\phi}^{n+1}$ into the above equation yields

$$\begin{aligned}
&\frac{gS_0}{2\Delta t}\left(\|\tilde{e}_{\phi}^{n+1}\|_p^2 - \|\tilde{e}_{\phi}^{n}\|_p^2 + \|\tilde{e}_{\phi}^{n+1}-\tilde{e}_{\phi}^{n}\|_p^2\right) + gK\|\nabla\tilde{e}_{\phi}^{n+1}\|_p^2\\
&= -R_{\phi}^{n+1}(\tilde{e}_{\phi}^{n+1}) + c_{\Gamma}(\mathbf{u}^n, \tilde{e}_{\phi}^{n+1}) - c_{\Gamma}(\mathbf{u}(t^{n+1}), \tilde{e}_{\phi}^{n+1}).
\end{aligned}$$

Using Cauchy-Schwarz and Young's inequalities, we have

$$|I_4| = |-R_{\phi}^{n+1}(\tilde{e}_{\phi}^{n+1})| \leq \epsilon_{\phi} gK\|\nabla\tilde{e}_{\phi}^{n+1}\|_p^2 + C\Delta t\int_{t^n}^{t^{n+1}} \|\partial_{tt}\phi\|_{-1,p}^2 dt,$$

$$\begin{aligned}
|I_5| &= |c_{\Gamma}(\mathbf{u}^n, \tilde{e}_{\phi}^{n+1}) - c_{\Gamma}(\mathbf{u}(t^{n+1}), \tilde{e}_{\phi}^{n+1})|\\
&\leq |c_{\Gamma}(e_{\mathbf{u}}^n, \tilde{e}_{\phi}^{n+1})| + |c_{\Gamma}(\mathbf{u}(t^{n+1}) - \mathbf{u}(t^n), \tilde{e}_{\phi}^{n+1})|\\
&\leq \epsilon_{\phi} gK\|\nabla\tilde{e}_{\phi}^{n+1}\|_p^2 + C\|\nabla e_{\mathbf{u}}^n\|_f\|e_{\mathbf{u}}^n\|_f + C\Delta t\int_{t^n}^{t^{n+1}} \|\partial_t\mathbf{u}\|_{1,f}^2 dt\\
&\leq \epsilon_{\phi} gK\|\nabla\tilde{e}_{\phi}^{n+1}\|_p^2 + C\|e_{\mathbf{u}}^n\|_f^2 + \frac{\epsilon_{\mathbf{u}}\nu}{C_1^2}\|\nabla e_{\mathbf{u}}^n\|_f^2 + C\Delta t\int_{t^n}^{t^{n+1}} \|\partial_t\mathbf{u}\|_{1,f}^2 dt.
\end{aligned}$$

Recalling (4.10)–(4.12), then we have the following result

$$\begin{aligned}
&\frac{gS_0}{2\Delta t}\left(\|\tilde{e}_{\phi}^{n+1}\|_p^2 - \|\tilde{e}_{\phi}^{n}\|_p^2 + \|\tilde{e}_{\phi}^{n+1}-\tilde{e}_{\phi}^{n}\|_p^2\right) + gK\|\nabla\tilde{e}_{\phi}^{n+1}\|_p^2\\
&\leq 2\epsilon_{\phi} gK\|\nabla\tilde{e}_{\phi}^{n+1}\|_p^2 + \epsilon_{\mathbf{u}}\nu\|\nabla\tilde{e}_{\mathbf{u}}^{n}\|_f^2 + C\|\tilde{e}_{\mathbf{u}}^{n}\|_f^2 + C\|\tilde{e}_{\phi}^{n}\|_p^2 + C|e_E^n|^2\\
&\quad + C\Delta t\int_{t^n}^{t^{n+1}} \|\partial_{tt}\phi\|_{-1,p}^2 dt + C\Delta t\int_{t^n}^{t^{n+1}} \|\partial_t\mathbf{u}\|_{1,f}^2 dt.
\end{aligned} \tag{4.15}$$

Adding (4.13) and (4.15) together, taking $\epsilon_{\mathbf{u}} = \frac{1}{8}$, $\epsilon_{\phi} = \frac{1}{6}$, summing them with n ranging from 0 to k, and then multiplying both sides by $2\Delta t$, we can obtain that

$$\begin{aligned}
&\|\tilde{e}_{\mathbf{u}}^{k+1}\|_f^2 + \sum_{n=0}^{k}\nu\Delta t\|\nabla\tilde{e}_{\mathbf{u}}^{n+1}\|_f^2 + \sum_{n=0}^{m}2\alpha\sqrt{\frac{\nu g}{tr(\mathbb{K})}}\Delta t\int_{\Gamma}(\tilde{e}_{\mathbf{u}}^{n+1}\cdot\boldsymbol{\tau})^2 ds + gS_0\|\tilde{e}_{\phi}^{k+1}\|_p^2 + \sum_{n=0}^{k} gK\Delta t\|\nabla\tilde{e}_{\phi}^{n+1}\|_p^2\\
&\leq \sum_{n=0}^{k}C\Delta t\|\tilde{e}_{\mathbf{u}}^{n}\|_f^2 + \sum_{n=0}^{k}C\Delta t\|\tilde{e}_{\phi}^{n}\|_p^2 + \sum_{n=0}^{k}C\Delta t|e_E^n|^2 + \sum_{n=0}^{k}C\Delta t\|\nabla e_{\mathbf{u}}^n\|_f^2\|\tilde{e}_{\mathbf{u}}^{n}\|_f^2\\
&\quad + \sum_{n=0}^{k}C\Delta t\|\nabla e_{\mathbf{u}}^n\|_f^2\|\tilde{e}_{\phi}^{n}\|_f^2 + \sum_{n=0}^{k}C\Delta t\|\nabla e_{\mathbf{u}}^n\|_f^2|e_E^n|^2 + \sum_{n=0}^{k}\Delta t\Big\{C\Delta t\int_{t^n}^{t^{n+1}}\|\partial_{tt}\mathbf{u}\|_{-1,f}^2 dt\\
&\quad + C\Delta t\int_{t^n}^{t^{n+1}}\|\partial_t\mathbf{u}\|_f^2 dt + C\Delta t\int_{t^n}^{t^{n+1}}\|\partial_t\mathbf{u}\|_{2,f}^2 dt + C\Delta t\int_{t^n}^{t^{n+1}}\|\partial_t\phi\|_{1,p}^2 dt\\
&\quad + C\Delta t\int_{t^n}^{t^{n+1}}\|\partial_{tt}\phi\|_{-1,p}^2 dt + C\Delta t\int_{t^n}^{t^{n+1}}\|\partial_t\mathbf{u}\|_{1,f}^2 dt\Big\}.
\end{aligned} \tag{4.16}$$

From the assumption (4.3) and Theorem 3.1, and applying the discrete Gronwall lemma, we have

$$\begin{aligned}
&\|\tilde{e}_{\mathbf{u}}^{k+1}\|_f^2 + \sum_{n=0}^{k}\nu\Delta t\|\nabla\tilde{e}_{\mathbf{u}}^{n+1}\|_f^2 + \sum_{n=0}^{m}2\alpha\sqrt{\frac{\nu g}{tr(\mathbb{K})}}\Delta t\int_{\Gamma}(\tilde{e}_{\mathbf{u}}^{n+1}\cdot\boldsymbol{\tau})^2 ds\\
&\qquad + gS_0\|\tilde{e}_{\phi}^{k+1}\|_p^2 + \sum_{n=0}^{k} gK\Delta t\|\nabla\tilde{e}_{\phi}^{n+1}\|_p^2 \leq C\Delta t^{2(1-\gamma)}.
\end{aligned} \tag{4.17}$$

Hence, when Δt is sufficiently small such that $\Delta t^{3/4-\gamma} \leq \hat{C}/C$, we obtain

$$\|\tilde{e}_{\mathbf{u}}^{k+1}\|_f + \|\tilde{e}_{\phi}^{k+1}\|_p \leq C\Delta t^{1-\gamma} \leq \hat{C}\Delta t^{\frac{1}{4}},$$

which completes the proof. □

4.2. A refined error estimate

Based on the rough error estimate established in Lemma 4.1, we shall use an induction process to derive a refined error analysis.

Theorem 4.2. *Given $1 \le k \le T/\Delta t - 1$, the following error estimate holds when Δt is sufficiently small*

$$|e_E^{k+1}| + \|\tilde{e}_{\mathbf{u}}^{k+1}\|_f + \|\tilde{e}_{\phi}^{k+1}\|_p \le C\Delta t, \tag{4.18}$$

$$\|e_{\mathbf{u}}^{k+1}\|_f + \|e_{\phi}^{k+1}\|_p \le C\Delta t. \tag{4.19}$$

Proof. We can easily obtain that (4.2) and (4.3) hold with $m = 0$. Next we assume that (4.2) and (4.3) hold for given $m = k$, $\forall 1 \le k \le T/\Delta t - 1$. Below, we shall prove that (4.2) and (4.3) hold for $m = k + 1$ with the same constants $\hat{C}$ and C^*.

For any $0 \le n \le k$, we derive from Lemma 4.1 that

$$0 < \frac{1}{2}E(t^{n+1}) \le \tilde{E}^{n+1} \le \frac{3}{2}E(t^{n+1}). \tag{4.20}$$

We also derive from (3.1) and (3.7) the following error equation for E:

$$\frac{e_E^{n+1} - e_E^n}{\Delta t} = \frac{dE(t^{n+1})}{dt} - \frac{E(t^{n+1}) - E(t^n)}{\Delta t} - \xi^{n+1}\mathbb{A}(\tilde{\mathbf{u}}^{n+1}, \tilde{\phi}^{n+1}) + \mathbb{A}(\mathbf{u}(t^{n+1}), \phi(t^{n+1})),$$

where $\mathbb{A}(\tilde{\mathbf{u}}^{n+1}, \tilde{\phi}^{n+1}) = \nu\|\nabla\tilde{\mathbf{u}}^{n+1}\|_f^2 + \alpha\sqrt{\frac{\nu g}{tr(\mathbb{K})}}\int_\Gamma(\tilde{\mathbf{u}}^{n+1}\cdot\boldsymbol{\tau})^2 ds + gK\|\nabla\tilde{\phi}^{n+1}\|_p^2$.

Multiplying both sides of the above equation by e_E^{n+1}, we obtain

$$\begin{aligned}
&\frac{1}{2\Delta t}\left(|e_E^{n+1}|^2 - |e_E^n|^2 + |e_E^{n+1} - e_E^n|^2\right)\\
&= (-\xi^{n+1}\mathbb{A}(\tilde{\mathbf{u}}^{n+1}, \tilde{\phi}^{n+1}) + \mathbb{A}(\mathbf{u}(t^{n+1}), \phi(t^{n+1})))e_E^{n+1} + \left(\frac{dE(t^{n+1})}{dt} - \frac{E(t^{n+1}) - E(t^n)}{\Delta t}\right)e_E^{n+1}\\
&\le C|e_E^{n+1}|^2 + C\Delta t\int_{t^n}^{t^{n+1}}|E_{tt}|^2 dt + I_6,
\end{aligned}$$

where

$$\begin{aligned}
I_6 &= \left|-\xi^{n+1}\mathbb{A}(\tilde{\mathbf{u}}^{n+1}, \tilde{\phi}^{n+1}) + \mathbb{A}(\mathbf{u}(t^{n+1}), \phi(t^{n+1}))\right||e_E^{n+1}|\\
&\le \left|\frac{E^{n+1}}{\tilde{E}^{n+1}}\left(\mathbb{A}(\tilde{\mathbf{u}}^{n+1}, \tilde{\phi}^{n+1}) - \mathbb{A}(\mathbf{u}(t^{n+1}), \phi(t^{n+1}))\right)\right|\left|e_E^{n+1}\right|\\
&\quad + \left|\mathbb{A}(\mathbf{u}(t^{n+1}), \phi(t^{n+1}))\left(1 - \frac{E^{n+1}}{\tilde{E}^{n+1}}\right)\right|\left|e_E^{n+1}\right| := I_{6,1} + I_{6,2}.
\end{aligned}$$

As indicated by (3.9), E^{n+1} is bounded with $E^{n+1} \le C$, and it follows from (4.20) that

$$\begin{aligned}
I_{6,1} &= \left|\frac{E^{n+1}}{\tilde{E}^{n+1}}\left(\mathbb{A}(\tilde{\mathbf{u}}^{n+1}, \tilde{\phi}^{n+1}) - \mathbb{A}(\mathbf{u}(t^{n+1}), \phi(t^{n+1}))\right)\right|\left|e_E^{n+1}\right|\\
&\le C\left|\left(\mathbb{A}(\tilde{\mathbf{u}}^{n+1}, \tilde{\phi}^{n+1}) - \mathbb{A}(\mathbf{u}(t^{n+1}), \phi(t^{n+1}))\right)\right|\left|e_E^{n+1}\right|\\
&\le C\left|\|\nabla\tilde{\mathbf{u}}^{n+1}\|_f + \|\nabla\mathbf{u}(t^{n+1})\|_f\right|\left\|\nabla\tilde{e}_{\mathbf{u}}^{n+1}\|_f\right|e_E^{n+1}\Big|\\
&\quad + C\left|\sqrt{\int_\Gamma(\tilde{\mathbf{u}}^{n+1}\cdot\boldsymbol{\tau})^2 ds} + \sqrt{\int_\Gamma(\mathbf{u}(t^{n+1})\cdot\boldsymbol{\tau})^2 ds}\right|\left|\sqrt{\int_\Gamma(\tilde{e}_{\mathbf{u}}^{n+1}\cdot\boldsymbol{\tau})^2 ds}\right|\left|e_E^{n+1}\right|\\
&\quad + C\left|\|\nabla\tilde{\phi}^{n+1}\|_p + \|\nabla\phi(t^{n+1})\|_p\right|\left\|\nabla\tilde{e}_{\phi}^{n+1}\|_p\right|e_E^{n+1}\Big|.
\end{aligned}$$

From the rough error estimate (4.17) and the regularity properties (4.1), we know that $\|\nabla\tilde{\mathbf{u}}^{n+1}\|_f^2$, $\int_\Gamma(\tilde{\mathbf{u}}^{n+1}\cdot\boldsymbol{\tau})^2 ds$ and $\|\nabla\tilde{\phi}^{n+1}\|_p^2$ are both bounded, so by applying the Cauchy-Schwarz and Young's inequalities, we have

$$I_{6,1} \le C\left|e_E^{n+1}\right|^2 + \epsilon_{\mathbf{u}}\nu\|\nabla\tilde{e}_{\mathbf{u}}^{n+1}\|_f^2 + \epsilon_\Gamma\alpha\sqrt{\frac{\nu g}{tr(\mathbb{K})}}\int_\Gamma(\tilde{e}_{\mathbf{u}}^{n+1}\cdot\boldsymbol{\tau})^2 ds + \epsilon_\phi gK\|\nabla\tilde{e}_{\phi}^{n+1}\|_p^2.$$

On the other hand,

$$\begin{aligned}
I_{6,2} &= \left|\mathbb{A}(\mathbf{u}(t^{n+1}), \phi(t^{n+1}))\left(1 - \frac{E^{n+1}}{\tilde{E}^{n+1}}\right)\right|\left|e_E^{n+1}\right|\\
&\le C\left|e_E^{n+1}\right|^2 + C\left|1 - \frac{E^{n+1}}{\tilde{E}^{n+1}}\right|^2\\
&\le C\left|e_E^{n+1}\right|^2 + C\|\tilde{e}_{\mathbf{u}}^{n+1}\|_f^2 + C\|\tilde{e}_{\phi}^{n+1}\|_p^2.
\end{aligned}$$

Combining the above inequalities, we obtain

$$\begin{aligned}
&\frac{1}{2\Delta t}\left(|e_E^{n+1}|^2-|e_E^{n}|^2+|e_E^{n+1}-e_E^{n}|^2\right)\\
&\le C|e_E^{n+1}|^2+\epsilon_{\mathbf{u}}\nu\|\nabla\tilde{e}_{\mathbf{u}}^{n+1}\|_f^2+\epsilon_\phi gK\|\nabla\tilde{e}_{\phi}^{n+1}\|_p^2+\epsilon_\Gamma\alpha\sqrt{\frac{\nu g}{tr(\mathbb{K})}}\int_\Gamma(\tilde{e}_{\mathbf{u}}^{n+1}\cdot\boldsymbol{\tau})^2ds\\
&\quad+C\|\tilde{e}_{\mathbf{u}}^{n+1}\|_f^2+C\|\tilde{e}_{\phi}^{n+1}\|_p^2+C\Delta t\int_{t^n}^{t^{n+1}}|E_{tt}|^2dt.
\end{aligned}\tag{4.21}$$

Adding (4.13), (4.15) and (4.21) together, setting $\epsilon_{\mathbf{u}}=\frac{1}{10}$, $\epsilon_\phi=\frac{1}{8}$, $\epsilon_\Gamma=\frac{1}{2}$, and summing them with n ranging from 0 to k, we arrive at

$$\begin{aligned}
&\|\tilde{e}_{\mathbf{u}}^{k+1}\|_f^2+\sum_{n=0}^{k}\nu\Delta t\|\nabla\tilde{e}_{\mathbf{u}}^{n+1}\|_f^2+\sum_{n=0}^{k}\alpha\sqrt{\frac{\nu g}{tr(\mathbb{K})}}\Delta t\int_\Gamma(\tilde{e}_{\mathbf{u}}^{n+1}\cdot\boldsymbol{\tau})^2ds+gS_0\|\tilde{e}_{\phi}^{k+1}\|_p^2\\
&+\sum_{n=0}^{k}gK\Delta t\|\nabla\tilde{e}_{\phi}^{n+1}\|_p^2+|e_E^{k+1}|^2\\
&\le\sum_{n=0}^{k}C\Delta t\|\tilde{e}_{\mathbf{u}}^{n}\|_f^2+\sum_{n=0}^{k}C\Delta t\|\tilde{e}_{\phi}^{n}\|_p^2+\sum_{n=0}^{k}C\Delta t|e_E^{n}|^2+\sum_{n=0}^{k}C\Delta t\|\nabla e_{\mathbf{u}}^{n}\|_f^2\|\tilde{e}_{\mathbf{u}}^{n}\|_f^2\\
&\quad+\sum_{n=0}^{k}C\Delta t\|\nabla e_{\mathbf{u}}^{n}\|_f^2\|\tilde{e}_{\phi}^{n}\|_f^2+\sum_{n=0}^{k}C\Delta t\|\nabla e_{\mathbf{u}}^{n}\|_f^2|e_E^{n}|^2+\sum_{n=0}^{k}C\Delta t|e_E^{n+1}|^2\\
&\quad+\sum_{n=0}^{k}C\Delta t\|\tilde{e}_{\mathbf{u}}^{n+1}\|_f^2+\sum_{n=0}^{k}C\Delta t\|\tilde{e}_{\phi}^{n+1}\|_p^2+\sum_{n=0}^{k}\Delta t\Big\{C\Delta t\int_{t^n}^{t^{n+1}}\|\partial_{tt}\mathbf{u}\|_{-1,f}^2dt\\
&\quad+C\Delta t\int_{t^n}^{t^{n+1}}\|\partial_t\mathbf{u}\|_f^2dt+C\Delta t\int_{t^n}^{t^{n+1}}\|\partial_t\mathbf{u}\|_{2,f}^2dt+C\Delta t\int_{t^n}^{t^{n+1}}\|\partial_t\phi\|_{1,p}^2dt\\
&\quad+C\Delta t\int_{t^n}^{t^{n+1}}\|\partial_{tt}\phi\|_{-1,p}^2dt+C\Delta t\int_{t^n}^{t^{n+1}}\|\partial_t\mathbf{u}\|_{1,f}^2dt+C\Delta t\int_{t^n}^{t^{n+1}}|E_{tt}|^2dt\Big\}.
\end{aligned}$$

Applying the discrete Gronwall lemma and using the regularity assumption to the above inequality, we obtain the desired result (4.18). Finally, recalling (4.9) and (4.10), we can obtain the error estimate (4.19).

It remains to verify that the assumptions (4.2) and (4.3) hold with $m=k+1$. For Δt is sufficiently small such that $\Delta t^{3/4}\le\hat{C}/C$ and $\Delta t^\gamma\le C^*/C$, we derive from (4.18) that

$$\begin{aligned}
&\|\tilde{e}_{\mathbf{u}}^{k+1}\|_f+gS_0\|\tilde{e}_{\phi}^{k+1}\|_p\le C\Delta t\le\hat{C}\Delta t^{1/4},\\
&|e_E^{k+1}|\le C\Delta t\le C^*\Delta t^{1-\gamma},\quad \gamma>0.
\end{aligned}$$

Hence the induction process is complete. □

5. Extension to the Cahn–Hilliard–Navier–Stokes–Darcy model

In this section, we extend the above linear and original-energy-dissipative scheme to the more complex Cahn–Hilliard–Navier–Stokes–Darcy model. While the Navier–Stokes–Darcy model is effective for single-phase scenarios, it cannot capture the interfacial dynamics inherent in two-phase flow, which is a limitation that the Cahn–Hilliard–Navier–Stokes–Darcy framework overcomes by introducing phase-field variables. This generalization provides a more comprehensive framework suitable for applications such as contaminant transport and enhanced oil recovery.

In the free-fluid domain Ω_f, the fluid is governed by the Cahn–Hilliard–Navier–Stokes equations [46,47].

$$\partial_t\mathbf{u}_f+(\mathbf{u}_f\cdot\nabla)\mathbf{u}_f-\nu_f\Delta\mathbf{u}_f+\nabla p_f+\phi_f\nabla\mu_f=0,\tag{5.1}$$

$$\nabla\cdot\mathbf{u}_f=0,\tag{5.2}$$

$$\partial_t\phi_f+\nabla\cdot(\mathbf{u}_f\phi_f)-\nabla\cdot(M(\phi_f)\nabla\mu_f)=0,\tag{5.3}$$

$$\mu_f+\lambda\epsilon\Delta\phi_f-\frac{\lambda}{\epsilon}G'(\phi_f)=0,\tag{5.4}$$

$$\mathbf{u}_f|_{\Gamma_f}=0,\qquad \mathbf{u}_f(\mathbf{x},0)=\mathbf{u}_f^0,\tag{5.5}$$

$$\nabla\phi_f\cdot\boldsymbol{n}|_{\Gamma_f}=0,\qquad \phi_f(\mathbf{x},0)=\phi_f^0,\tag{5.6}$$

$$M(\phi_f)\nabla\mu_f\cdot\boldsymbol{n}|_{\Gamma_f}=0,\qquad \mu_f(\mathbf{x},0)=\mu_f^0,\tag{5.7}$$

where $\mathbf{u}_f$ and p_f are the velocity and pressure of the free flow, respectively. The phase field function is ϕ_i $(i=f,p)$, and the corresponding chemical potential is μ_i $(i=f,p)$. The free energy $G(\phi)$ is defined by a double-well polynomial, $G(\phi)=\frac{1}{4}(\phi^2-1)^2$. Here, ν_i

($i = f, p$) is the kinematic viscosity, ϵ denotes the interfacial width, $M(\phi_i)$ ($i = f, p$) is the mobility related to ϕ_i, and λ is the elastic relaxation time.

In the porous-media domain Ω_p, the fluid satisfies the Cahn–Hilliard–Darcy equations [48,49].

$$\chi^{-1}\partial_t \mathbf{u}_p + \mathbb{K}^{-1}\mathbf{u}_p + \nabla p_p + \phi_p \nabla \mu_p = 0, \tag{5.8}$$

$$\nabla \cdot \mathbf{u}_p = 0, \tag{5.9}$$

$$\partial_t \phi_p + \nabla \cdot (\mathbf{u}_p \phi_p) - \nabla \cdot (M(\phi_p)\nabla \mu_p) = 0, \tag{5.10}$$

$$\mu_p + \lambda\epsilon\Delta\phi_p - \frac{\lambda}{\epsilon}G'(\phi_p) = 0, \tag{5.11}$$

$$\mathbf{u}_p \cdot \boldsymbol{n}|_{\Gamma_p} = 0, \qquad \mathbf{u}_p(\mathbf{x}, 0) = \mathbf{u}_p^0, \tag{5.12}$$

$$\nabla\phi_p \cdot \boldsymbol{n}|_{\Gamma_p} = 0, \qquad \phi_p(\mathbf{x}, 0) = \phi_p^0, \tag{5.13}$$

$$M(\phi_p)\nabla\mu_p \cdot \boldsymbol{n}|_{\Gamma_p} = 0, \qquad \mu_p(\mathbf{x}, 0) = \mu_p^0, \tag{5.14}$$

where $\mathbf{u}_p$ is the velocity, p_p is the hydraulic head, $\mathbb{K}$ is the hydraulic conductivity tensor. χ represents the porosity of porous media.

The interface conditions are defined as follows.

$$\phi_f = \phi_p, \qquad \nabla\phi_f \cdot \boldsymbol{n} = \nabla\phi_p \cdot \boldsymbol{n}, \tag{5.15}$$

$$\mu_f = \mu_p, \qquad M(\phi_f)\nabla w_f \cdot \boldsymbol{n} = M(\phi_p)\nabla w_p \cdot \boldsymbol{n}, \tag{5.16}$$

$$\mathbf{u}_f \cdot \mathbf{n} = \mathbf{u}_p \cdot \mathbf{n}, \tag{5.17}$$

$$p_f - \nu_f \mathbf{n} \cdot (\nabla \mathbf{u}_f \cdot \mathbf{n}) + \frac{1}{2}|\mathbf{u}_f|^2 = p_p, \tag{5.18}$$

$$-\nu_f \boldsymbol{\tau} \cdot (\nabla \mathbf{u}_f \cdot \mathbf{n}) = \frac{\alpha\nu_f\sqrt{d}}{\sqrt{\nu_p tr(\mathbb{K})}}(\mathbf{u}_f \cdot \boldsymbol{\tau}). \tag{5.19}$$

We also define the following spaces:

$$X_f = \{\mathbf{v} \in (H^1(\Omega_f))^d : \mathbf{v}|_{\Gamma_f} = 0\}, \qquad X_p = \{\mathbf{v} \in (H^1(\Omega_p))^d : \mathbf{v}\cdot\boldsymbol{n}|_{\Gamma_p} = 0\},$$
$$M_f = L^2(\Omega_f), \qquad M_p = \{q \in H^1(\Omega_p) : \int_{\Omega_p} q d\mathbf{x} = 0\}, \qquad Y = H^1(\Omega).$$

Then, a weak formulation for the above system is: Find $(\mathbf{u}_f, p_f, \mathbf{u}_p, p_p, \phi, w) \in (X_f \times M_f \times X_p \times M_p \times Y \times Y)$ such that for all $(\mathbf{v}_f, q_f, \mathbf{v}_p, q_p, \psi, \omega) \in (X_f \times M_f \times X_p \times M_p \times Y \times Y)$,

$$(\partial_t\phi, \psi) - (\mathbf{u}\phi, \nabla\psi) + (M(\phi)\nabla\mu, \nabla\psi) = 0, \tag{5.20}$$

$$(\mu, \omega) - \lambda\epsilon(\nabla\phi, \nabla\omega) - \frac{\lambda}{\epsilon}(G'(\phi), \omega) = 0, \tag{5.21}$$

$$\chi^{-1}(\partial_t\mathbf{u}_p, \mathbf{v}_p)_p + \mathbb{K}^{-1}(\mathbf{u}_p, \mathbf{v}_p)_p + (\nabla p_p, \mathbf{v}_p)_p + (\phi_p\nabla\mu_p, \mathbf{v}_p)_p = 0, \tag{5.22}$$

$$-(\mathbf{u}_p, \nabla q_p)_p - \int_\Gamma (\mathbf{u}_f \cdot \mathbf{n}) q_p ds = 0, \tag{5.23}$$

$$\begin{aligned}&(\frac{\partial \mathbf{u}_f}{\partial t}, \mathbf{v}_f)_f + a(\mathbf{u}_f, \mathbf{u}_f, \mathbf{v}_f) + \nu_f(\nabla\mathbf{u}_f, \nabla\mathbf{v}_f)_f - (p_f, \nabla\cdot\mathbf{v}_f)_f + \int_\Gamma p_p(\mathbf{v}_f\cdot\mathbf{n})ds \\ &\quad + \frac{\alpha\nu_f\sqrt{d}}{\sqrt{\nu_p tr(\mathbb{K})}}\int_\Gamma (\mathbf{u}_f\cdot\boldsymbol{\tau})(\mathbf{v}_f\cdot\boldsymbol{\tau})ds + (\phi_f\nabla\mu_f, \mathbf{v}_f)_f = 0,\end{aligned} \tag{5.24}$$

$$(\nabla\cdot\mathbf{u}_f, q_f)_f = 0. \tag{5.25}$$

It is easy to verify that the above Cahn–Hilliard–Navier–Stokes–Darcy model satisfies the following energy dissipation law

$$\frac{dE}{dt} = -\nu_f\|\nabla\mathbf{u}_f\|_f^2 + \frac{\alpha\nu_f\sqrt{d}}{\sqrt{\nu_p tr(\mathbb{K})}}\int_\Gamma (\mathbf{u}_f\cdot\boldsymbol{\tau})^2 ds + \|\sqrt{\mathbb{K}^{-1}}\mathbf{u}_p\|_p^2 + M(\phi)\|\nabla\mu\|^2,$$

where the original energy is defined as

$$E = \left(\frac{\lambda\epsilon}{2}\|\nabla\phi\|^2 + \frac{\lambda}{\epsilon}\int_\Omega G(\phi)d\mathbf{x}\right) + \left(\frac{1}{2}\|\mathbf{u}_f\|_f^2 + \frac{1}{2\chi}\|\mathbf{u}_p\|_p^2\right) := E_0 + E_1.$$

In order to construct efficient and unconditionally energy stable schemes for the Cahn–Hilliard–Navier–Stokes–Darcy model, we introduce a scalar auxiliary variable $\xi(t) \equiv 1$, which serves as a relaxation factor, and expand the model with a reformulated energy dissipation law:

$$\frac{dE}{dt} = \xi(t)\left(-\nu_f\|\nabla\mathbf{u}_f\|_f^2 + \frac{\alpha\nu_f\sqrt{d}}{\sqrt{\nu_p tr(\mathbb{K})}}\int_\Gamma (\mathbf{u}_f\cdot\boldsymbol{\tau})^2 ds + \|\sqrt{\mathbb{K}^{-1}}\mathbf{u}_p\|_p^2 + M(\phi)\|\nabla\mu\|^2\right). \tag{5.26}$$

Then, following essentially the same principle as **Scheme I**, we construct below a first-order scheme for the expanded system of (5.20)–(5.25) with (5.26).

Scheme III: a first-order scheme for the Cahn–Hilliard–Navier–Stokes–Darcy model.

Step 1 (Prediction). Find $(\phi^{n+1}, \mu^{n+1}) \in (Y \times Y)$ such that

$$\left(\frac{\phi^{n+1}-\phi^n}{\Delta t}, \psi\right) - (\mathbf{u}^n\phi^n, \nabla\psi) + (M(\phi^n)\nabla\mu^{n+1}, \nabla\psi) = 0, \tag{5.27}$$

$$(\mu^{n+1}, \omega) - \lambda\epsilon(\nabla\phi^{n+1}, \nabla\omega) - \frac{\lambda}{\epsilon}(G'(\phi^n), \omega) = 0. \tag{5.28}$$

Find $(\tilde{\mathbf{u}}_p^{n+1}, p_p^{n+1}) \in (X_p \times M_p)$ such that

$$\chi^{-1}\left(\frac{\tilde{\mathbf{u}}_p^{n+1}-\tilde{\mathbf{u}}_p^n}{\Delta t}, \mathbf{v}_p\right)_p + \mathbb{K}^{-1}(\tilde{\mathbf{u}}_p^{n+1}, \mathbf{v}_p)_p + (\nabla p_p^{n+1}, \mathbf{v}_p)_p + (\phi_p^{n+1}\nabla\mu_p^{n+1}, \mathbf{v}_p)_p = 0, \tag{5.29}$$

$$-(\tilde{\mathbf{u}}_p^{n+1}, \nabla q_p)_p - \int_\Gamma (\mathbf{u}_f^n \cdot \mathbf{n}) q_p ds = 0. \tag{5.30}$$

Find $(\tilde{\mathbf{u}}_f^{n+1}, p_f^{n+1}) \in (X_f \times M_f)$ such that

$$\begin{aligned}&\left(\frac{\tilde{\mathbf{u}}_f^{n+1}-\tilde{\mathbf{u}}_f^n}{\Delta t}, \mathbf{v}_f\right)_f + a(\mathbf{u}_f^n, \mathbf{u}_f^n, \mathbf{v}_f) + \nu_f(\nabla\tilde{\mathbf{u}}_f^{n+1}, \nabla\mathbf{v}_f)_f - (p_f^{n+1}, \nabla\cdot\mathbf{v}_f)_f + \int_\Gamma p_p^{n+1}(\mathbf{v}_f\cdot\mathbf{n})ds\\ &\quad + \frac{\alpha\nu_f\sqrt{d}}{\sqrt{\nu_p tr(\mathbb{K})}}\int_\Gamma (\tilde{\mathbf{u}}_f^{n+1}\cdot\boldsymbol{\tau})(\mathbf{v}_f\cdot\boldsymbol{\tau})ds + (\phi_f^{n+1}\nabla\mu_f^{n+1}, \mathbf{v}_f)_f = 0,\end{aligned} \tag{5.31}$$

$$(\nabla\cdot\tilde{\mathbf{u}}_f^{n+1}, q_f)_f = 0. \tag{5.32}$$

Step 2 (Correction). We denote

$$\tilde{E}^{n+1} = \left(\frac{\lambda\epsilon}{2}\|\nabla\phi^{n+1}\|^2 + \frac{\lambda}{\epsilon}\int_\Omega G(\phi^{n+1})d\mathbf{x}\right) + \left(\frac{1}{2}\|\tilde{\mathbf{u}}_f^{n+1}\|_f^2 + \frac{1}{2\chi}\|\tilde{\mathbf{u}}_p^{n+1}\|_p^2\right) := E_0^{n+1} + \tilde{E}_1^{n+1}, \tag{5.33}$$

and set

$$E^{n+1} = E_0^{n+1} + \xi^{n+1}\tilde{E}_1^{n+1}. \tag{5.34}$$

Then, we determine ξ^{n+1} from the linear algebraic equation

$$\begin{aligned}\frac{E^{n+1}-E^n}{\Delta t} &= -\xi^{n+1}\Big(\nu_f\|\nabla\tilde{\mathbf{u}}_f^{n+1}\|_f^2 + \frac{\alpha\nu_f\sqrt{d}}{\sqrt{\nu_p tr(\mathbb{K})}}\int_\Gamma (\tilde{\mathbf{u}}_f^{n+1}\cdot\boldsymbol{\tau})^2 ds\\ &\qquad + \|\sqrt{\mathbb{K}^{-1}}\tilde{\mathbf{u}}_p^{n+1}\|_p^2 + M(\phi^{n+1})\|\nabla\mu^{n+1}\|^2\Big).\end{aligned} \tag{5.35}$$

Finally, we set

$$\mathbf{u}_f^{n+1} = \sqrt{\xi^{n+1}}\tilde{\mathbf{u}}_f^{n+1}, \qquad \mathbf{u}_p^{n+1} = \sqrt{\xi^{n+1}}\tilde{\mathbf{u}}_p^{n+1}. \tag{5.36}$$

Similarly, a linear and second-order version of **Scheme III** can be constructed to preserve the dissipation of the original energy. Following a similar approach to the proof of Theorem 3.1, we can establish the following stability result for **Scheme III**:

Theorem 5.1. *The scheme (5.27)–(5.36) dissipates the original energy as shown by (5.35). Moreover, we have*

$$\begin{aligned}&\frac{\lambda\epsilon}{2}\|\nabla\phi^{k+1}\|^2 + \frac{\lambda}{\epsilon}\int_\Omega G(\phi^{k+1})d\mathbf{x} + \frac{1}{2}\|\mathbf{u}_f^{k+1}\|_f^2 + \frac{1}{2\chi}\|\mathbf{u}_p^{k+1}\|_p^2 + \Delta t\sum_{n=0}^{k}\Big(\nu_f\|\nabla\mathbf{u}_f^{n+1}\|_f^2\\ &\quad + \frac{\alpha\nu_f\sqrt{d}}{\sqrt{\nu_p tr(\mathbb{K})}}\int_\Gamma (\mathbf{u}_f^{n+1}\cdot\boldsymbol{\tau})^2 ds + \|\sqrt{\mathbb{K}^{-1}}\mathbf{u}_p^{n+1}\|_p^2\Big) \le C,\end{aligned} \tag{5.37}$$

where C is a positive constant depending on the initial conditions $\phi^0, \mathbf{u}_f^0, \mathbf{u}_p^0$. Here we assume $\xi^{n+1} \ge 0$.

Proof. From (5.35), we can derive that

$$\frac{E^{n+1}-E^n}{\Delta t} = -\xi^{n+1}\mathbb{F}(\tilde{\mathbf{u}}_f^{n+1}, \tilde{\mathbf{u}}_p^{n+1}, \phi^{n+1}, \mu^{n+1}) \le 0,$$

where

$$\begin{aligned}\mathbb{F}(\tilde{\mathbf{u}}_f^{n+1}, \tilde{\mathbf{u}}_p^{n+1}, \phi^{n+1}, \mu^{n+1}) &= \nu_f\|\nabla\tilde{\mathbf{u}}_f^{n+1}\|_f^2 + \frac{\alpha\nu_f\sqrt{d}}{\sqrt{\nu_p tr(\mathbb{K})}}\int_\Gamma (\tilde{\mathbf{u}}_f^{n+1}\cdot\boldsymbol{\tau})^2 ds\\ &\quad + \|\sqrt{\mathbb{K}^{-1}}\tilde{\mathbf{u}}_p^{n+1}\|_p^2 + M(\phi^{n+1})\|\nabla\mu^{n+1}\|^2\end{aligned} \tag{5.38}$$

$$\geq 0.$$

Also, by summing up (5.38) from $n = 0$ to $n = k$, we have

$$E^{k+1} + \Delta t \sum_{n=0}^{k} \xi^{n+1} \mathbb{F}(\tilde{\mathbf{u}}_f^{n+1}, \tilde{\mathbf{u}}_p^{n+1}, \phi^{n+1}, \mu^{n+1}) = E^0 \leq C,$$

which implies (5.37).

□

6. Numerical experiments

In order to validate the essential properties of the numerical schemes proposed in this paper, we conduct six numerical tests that focus on different aspects of the schemes. We choose Taylor-Hood elements (**P**2-P1) for the velocity and pressure of free flow and P2 finite element for the flow in the porous-media domain. For the two-phase flow, we choose P1 finite element for both phase function and chemical potential. All numerical experiments presented below are conducted using a uniform mesh and the open-source finite element software package FreeFem + + [50].

6.1. The EMAC formulation

It is noted in [51] that if the discrete velocity approximation is not exactly divergence free, errors for the conserved quantities, such as mass, momentum, and angular momentum, may accumulate rapidly overtime. The EMAC formulation, originally proposed for the Navier–Stokes equations in [52], can preserve energy, momentum, and angular momentum in a discrete setting. Since the Taylor-Hood elements do not lead to exactly divergence free velocity approximation, we shall adapt the EMAC formulation which is presented below.

As proposed in [51], we introduce $P = p - \frac{1}{2}|\mathbf{u}|^2$ and present an equivalent form for the convective term and pressure in the Navier–Stokes equations.

$$\mathbf{u} \cdot \nabla \mathbf{u} + \nabla p = 2\mathbb{D}(\mathbf{u})\mathbf{u} + (\nabla \cdot \mathbf{u})\mathbf{u} + \nabla P,$$

where the strain tensor $\mathbb{D}(\mathbf{u}) = \frac{1}{2}(\nabla \mathbf{u} + (\nabla \mathbf{u})^T)$. Similarly, we derive the weak form with the EMAC formulation for the problems defined by Eqs. (2.1)–(2.10). For $\forall\, t \in (0, T]$, find $\mathbf{u} \in H_f,\ P \in Q_f,\ \phi \in H_p$ such that

$$\begin{cases} (\partial_t \mathbf{u}, \mathbf{v})_f + gS_0(\partial_t \phi, \psi)_p + \nu(\nabla \mathbf{u}, \nabla \mathbf{v})_f - (P, \nabla \cdot \mathbf{v})_f + b(\mathbf{u}, \mathbf{u}, \mathbf{v}) + \alpha \sqrt{\dfrac{\nu g}{tr(\mathbb{K})}} \displaystyle\int_\Gamma (\mathbf{u} \cdot \boldsymbol{\tau})(\mathbf{v} \cdot \boldsymbol{\tau}) ds \\ \qquad + g(\mathbb{K}\nabla \phi, \nabla \psi)_p + c_\Gamma(\mathbf{v}, \phi) - c_\Gamma(\mathbf{u}, \psi) = (\mathbf{f}_f, \mathbf{v})_f + g(f_p, \psi)_p, \qquad \forall \mathbf{v} \in H_f,\ \psi \in H_p, \\ (\nabla \cdot \mathbf{u}, q)_f = 0, \qquad \forall q \in Q_f, \\ (\mathbf{u}(\mathbf{x}, 0), \mathbf{v})_f = (\mathbf{u}^0, \mathbf{v})_f, \qquad \forall \mathbf{v} \in H_f, \\ (\phi(\mathbf{x}, 0), \psi)_p = (\phi^0, \psi)_p, \qquad \forall \psi \in H_p, \end{cases} \tag{6.1}$$

where

$$b(\mathbf{u}, \mathbf{v}, \mathbf{w}) = (2\mathbb{D}(\mathbf{u})\mathbf{v}, \mathbf{w})_f + ((\nabla \cdot \mathbf{u})\mathbf{v}, \mathbf{w})_f - \int_\Gamma (\mathbf{u} \cdot \mathbf{v})(\mathbf{w} \cdot \mathbf{n}) ds, \qquad \forall \mathbf{u}, \mathbf{v}, \mathbf{w} \in H_f,$$

$$c_\Gamma(\mathbf{v}, \phi) = g \int_\Gamma \phi \mathbf{v} \cdot \mathbf{n} ds, \qquad \forall \mathbf{v} \in H_f,\ \phi \in H_p.$$

Lemma 6.1. *The nonlinear term $b(\mathbf{u}, \mathbf{v}, \mathbf{w})$ has the following property:*

$$b(\mathbf{u}, \mathbf{u}, \mathbf{u}) = 0, \quad \forall \mathbf{u} \in H_f. \tag{6.2}$$

Proof. Since the nonlinear term $b(\mathbf{u}, \mathbf{u}, \mathbf{u}) = (2\mathbb{D}(\mathbf{u})\mathbf{u}, \mathbf{u})_f + ((\nabla \cdot \mathbf{u})\mathbf{u}, \mathbf{u})_f - \int_\Gamma (\mathbf{u} \cdot \mathbf{u})(\mathbf{u} \cdot \mathbf{n}) ds$, by using the Green's formula, we can obtain

$$\begin{aligned} b(\mathbf{u}, \mathbf{u}, \mathbf{u}) &= (2\mathbb{D}(\mathbf{u})\mathbf{u}, \mathbf{u})_f - (\mathbf{u}, \nabla(\mathbf{u} \cdot \mathbf{u}))_f + \int_\Gamma (\mathbf{u} \cdot \mathbf{u})(\mathbf{u} \cdot \mathbf{n}) ds - \int_\Gamma (\mathbf{u} \cdot \mathbf{u})(\mathbf{u} \cdot \mathbf{n}) ds \\ &= (2(\nabla \mathbf{u})\mathbf{u}, \mathbf{u})_f - (2(\nabla \mathbf{u})\mathbf{u}, \mathbf{u})_f + \int_\Gamma (\mathbf{u} \cdot \mathbf{u})(\mathbf{u} \cdot \mathbf{n}) ds - \int_\Gamma (\mathbf{u} \cdot \mathbf{u})(\mathbf{u} \cdot \mathbf{n}) ds \\ &= 0, \qquad \forall \mathbf{u} \in H_f. \end{aligned}$$

□

Remark 6.1. We can replace the trilinear form $a(\cdot, \cdot, \cdot)$ and $(p^{n+1}, \nabla \cdot \mathbf{v})_f$ in **Schemes I, II and III** by $b(\cdot, \cdot, \cdot)$ and $(P^{n+1}, \nabla \cdot \mathbf{v})_f$ to obtain the corresponding EMAC schemes. It should be noted that the stability results established for **Schemes I, II and III** are also valid for the corresponding EMAC schemes. However, the error analysis will require further effort.

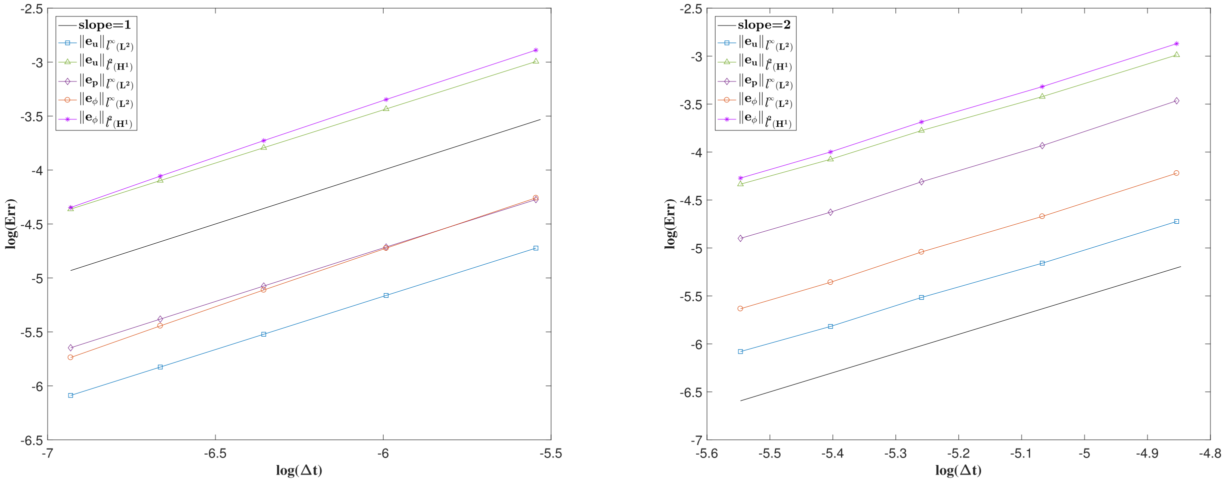

Fig. 1. Comparison of numerical errors and convergence rates with $T = 0.5$ (Example 1). Left: **Scheme I**, right: **Scheme II**.

6.2. Example 1: Convergence tests A

We first set the parameters $\nu = 0.001$, $\mathbb{K} = \mathbb{J}$ and all other parameters to 1. We choose the computational domain as $\Omega_f = (0,1)\times(0,1)$, $\Omega_p = (0,1)\times(-1,0)$. The exact solution, along with the corresponding initial values and source terms, is constructed as follows.

$$\begin{cases} \mathbf{u} = [\mathbf{u}_1, \mathbf{u}_2] = [x^2y^2\cos(t), -\frac{2}{3}xy^3\cos(t)], \\ p = cx^2(x-1)^2y^2(y-1)^2\cos(t), \\ \phi = cx^2(x-1)^2(y+1)^2y^2\cos(t). \end{cases}$$

We set $c = 64\pi^2$ and consider a series of spatial mesh sizes $h = 1/16, 1/20, 1/24, 1/28, 1/32$ with the time step $\Delta t = h^2$. The corresponding numerical results are presented in Fig. 1. As shown in Fig. 1, the convergence order achieves first order, which is in consistent with Theorem 4.2. Subsequently, we set $\Delta t = h/8$ to examine the performance of **Scheme II**. These results, also shown in Fig. 1, clearly demonstrate second-order temporal accuracy.

6.3. Example 2: Convergence tests B

In this example, all parameters are kept identical to those in Example 1. The analytic solution is chosen as

$$\begin{cases} \mathbf{u} = [\mathbf{u}_1, \mathbf{u}_2] = \left[l\sin^2(\pi x)\sin(2\pi y)\cos(t), -l\sin(2\pi x)\sin^2(\pi y)\cos(t)\right], \\ p = \sin(\pi y)\cos(\pi x)\cos(t), \\ \phi = \sin(\pi x)\sin^2(\pi y)\cos(t). \end{cases}$$

The numerical results using **Scheme I** with $l = 1/20\pi^2$, $h = 1/16, 1/20, 1/24, 1/28, 1/32$, and $\Delta t = h^2$, are presented in Fig. 2. We can easily obtain the temporal convergence order of the first-order scheme. Then we set $\Delta t = h/4$ to explore the convergence rate of **Scheme II**, the desired results also provided in Fig. 2.

6.4. Example 3: Numerical simulation of filtration flows

In this example, we study the impact of different hydraulic conductivities on free flow within porous media, which can be regarded as a simple simulation of a filter. In particular, we will choose various location and length of the low hydraulic conductivity regions on porous media by using **Scheme II** with EMAC formulation. We set the computational domain as $\Omega_f = (0,2)\times(1.5,2)$, $\Omega_p = (0,2)\times(0,1.5)$ and $\Gamma = (0,2)\times\{1.5\}$ with final time $T = 0.5$, $\Delta t = 0.005$, $h = 1/80$, and other parameters all be 1. The initial conditions are given as $\mathbf{u}_f^0 = (0, 0.015x(x-2))$, $\phi^0 = 0$.

The following configurations are prescribed: For cases (a)-(f), the hydraulic conductivity is set to $K = 10^{-6}$ within two small rectangular subdomains and $K = 1$ elsewhere. For case (g), the hydraulic conductivity tensor is defined as

$$\mathbb{K} = \begin{bmatrix} \mathrm{rand}(x,y) & 0.1\mathrm{rand}(x,y) \\ 0.1\mathrm{rand}(x,y) & \mathrm{rand}(x,y) \end{bmatrix},$$

where $\mathrm{rand}(x,y)$ denotes a uniformly distributed random variable on the interval $(0,1]$.

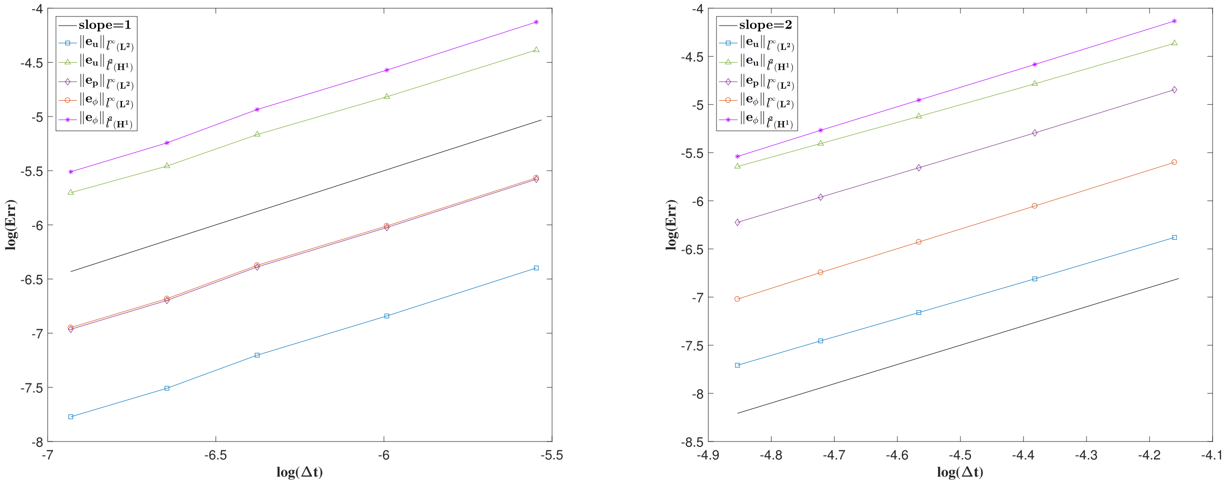

Fig. 2. Comparison of numerical errors and convergence rates with $T = 0.5$ (Example 2). Left: **Scheme I**, right: **Scheme II**.

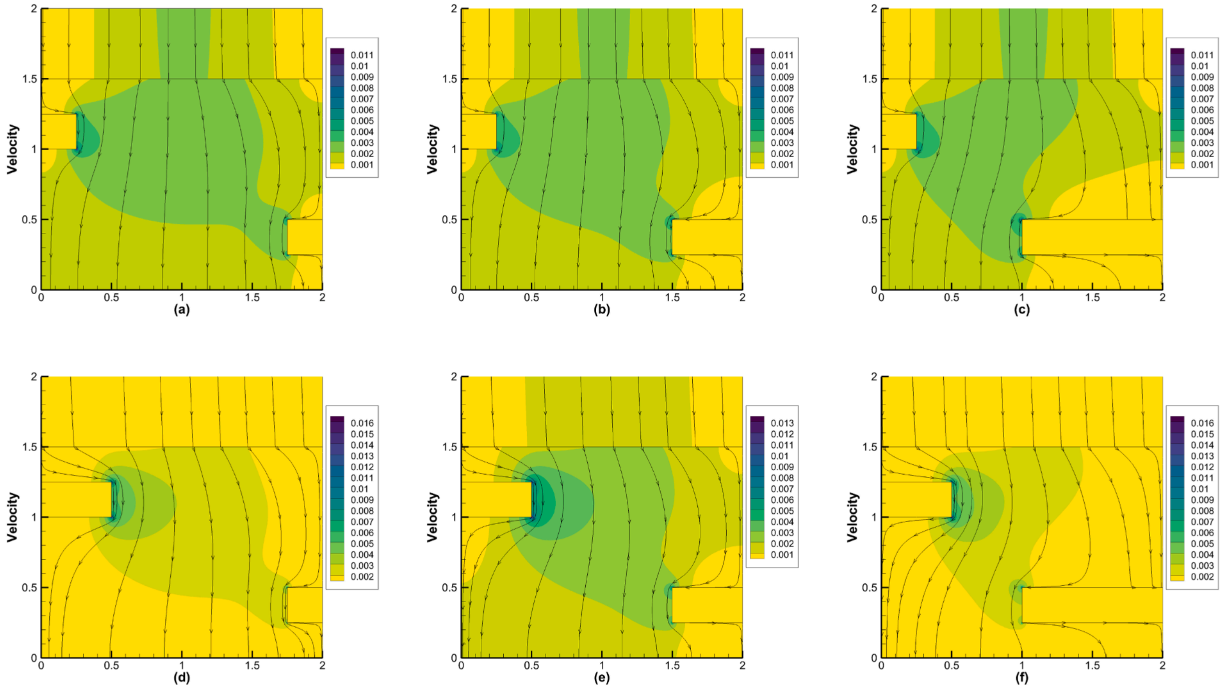

Fig. 3. Comparison of velocity field distributions driven by initial velocity in different porous-media configurations (**Scheme II**).

In Fig. 3 and Fig. 4, we illustrate the fluid flow path and pressure field distributions driven by initial velocity with the diagonal hydraulic conductivity tensor in different porous-media configurations. Fig. 5 displays the velocity streamlines and pressure field with the random hydraulic conductivity tensor. As shown in these figures, upon encountering the first low hydraulic conductivity region, the flow aligns with the region's geometry, exhibiting localized velocity increases near its corners. A comparable flow pattern, including corner acceleration, occurs within the second low hydraulic conductivity region. Horizontal comparisons, achieved by fixing the width of the first region and varying the width of the second rectangular region, demonstrate that the magnitude of the velocity increase near the corners, which becomes more pronounced as the width of the low hydraulic conductivity region increases. Vertical comparisons yield similar results. This observed behavior is consistent with the Venturi effect in fluid dynamics, which aligns with the results documented in [53,54] regarding flow through constrictions. From Fig. 6, we can see that ξ remains consistently close to 1 and the original energy dissipative with various settings.

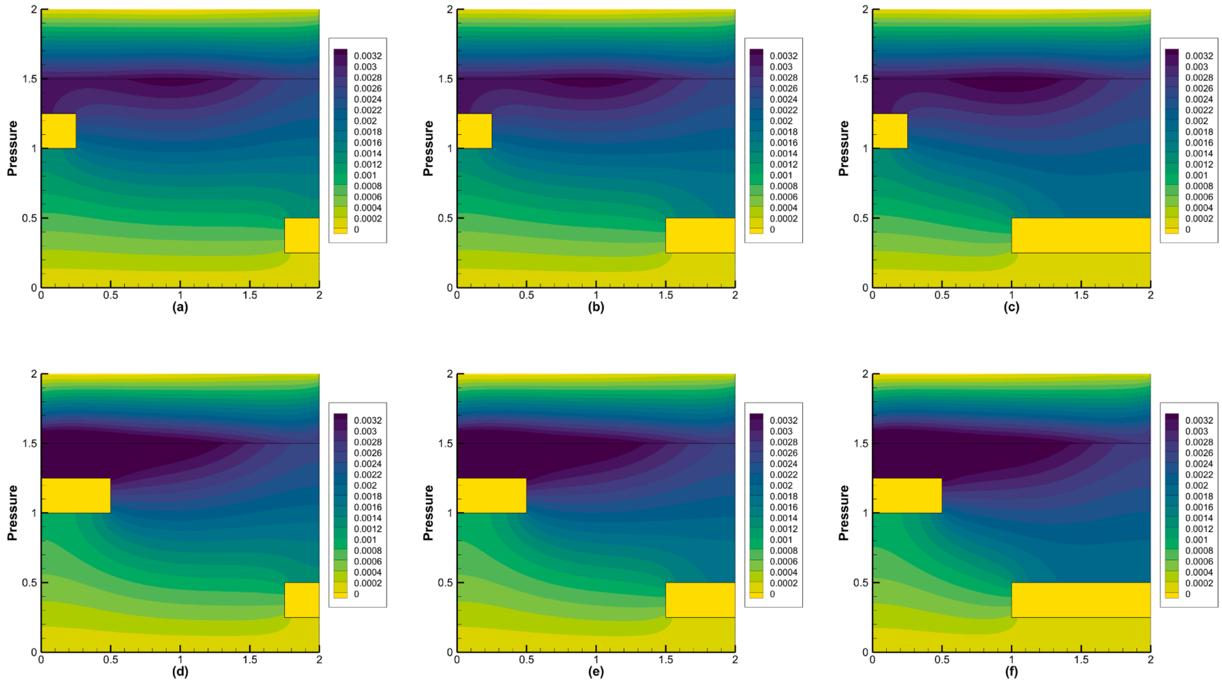

Fig. 4. Comparison of pressure field distributions driven by initial velocity in different porous-media configurations (**Scheme II**).

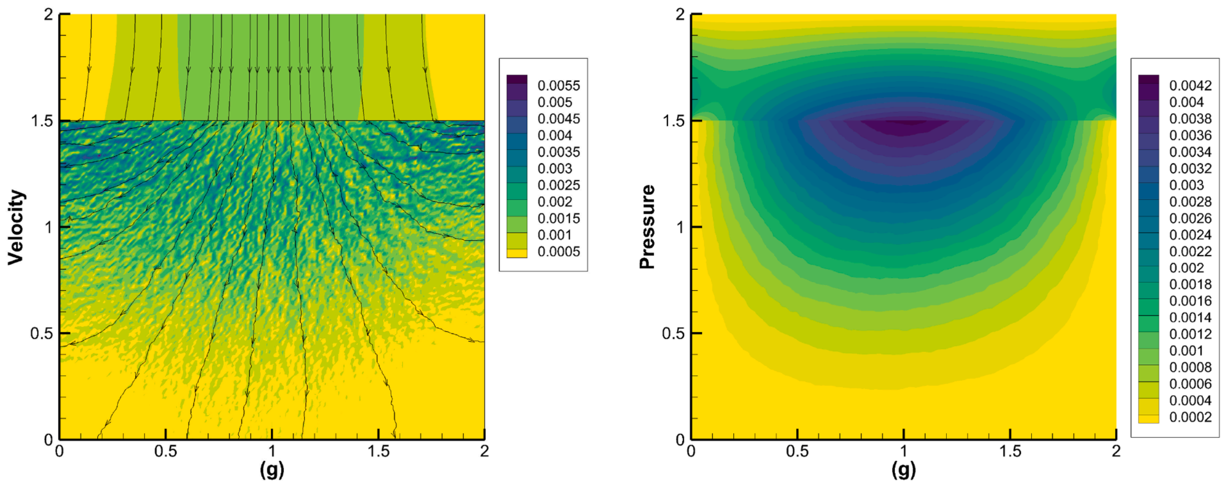

Fig. 5. Left: velocity field distribution, right: pressure field distribution, for a random hydraulic conductivity tensor.

6.5. Example 4: Phase separation dynamics with random initial conditions

In this numerical example, we validate **Scheme III** with EMAC formulation by simulating phase separation dynamics for the Cahn–Hilliard–Navier–Stokes–Darcy model. The initial phase field variable is set to

$$\phi^0 = y - 1 + 0.01 rand(x, y),$$

where $rand(x, y)$ denotes a uniformly distributed random variable on $[-1, 1]$, with parameters $\Delta t = 0.0005$, $h = 1/100$, $\nu_f = \nu_p = 0.1$, $\alpha = 0.01$, $\chi = 1$, $\lambda = 0.1$, $M(\phi) = \epsilon\sqrt{(1-\phi)^2 + \epsilon^2}$, $\epsilon = 0.01$, and hydraulic conductivity tensor

$$\mathbb{K} = \begin{bmatrix} 0.5 & 0.1 \\ 0.1 & 0.2 \end{bmatrix}.$$

The computational domain $\Omega = (0, 1) \times (0, 2)$ includes a free-flow region $\Omega_f = (0, 1) \times (0, 1)$ and a porous-media region $\Omega_p = (0, 1) \times (1, 2)$.

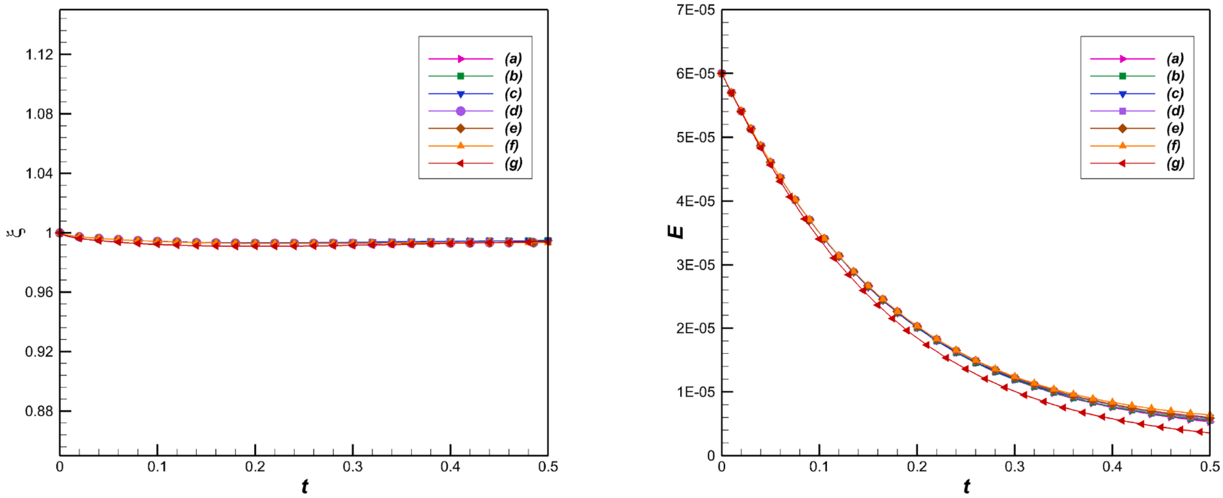

Fig. 6. Evolution of key quantities. Left: relaxation factor ξ, right: original energy E (Example 3).

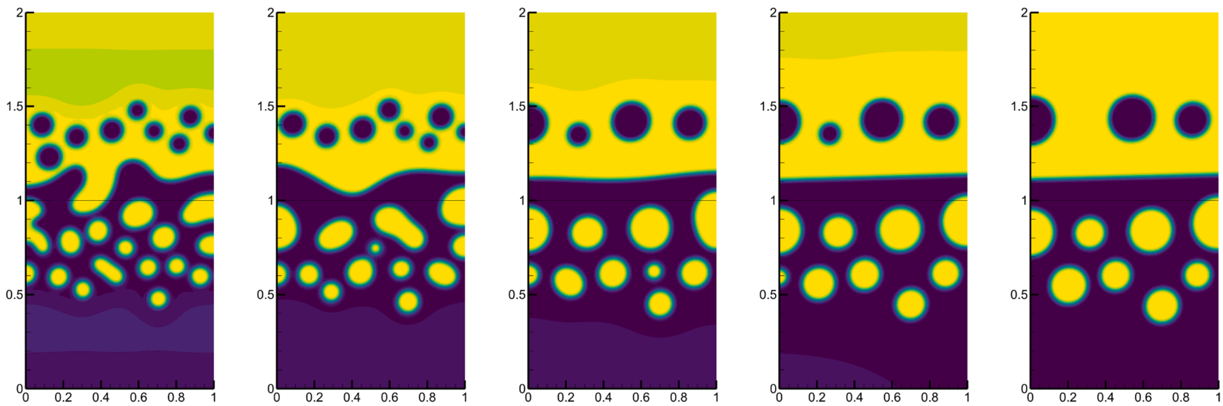

Fig. 7. Phase-field evolution from random initial conditions at T = 0.5, 1, 2, 4, 10.

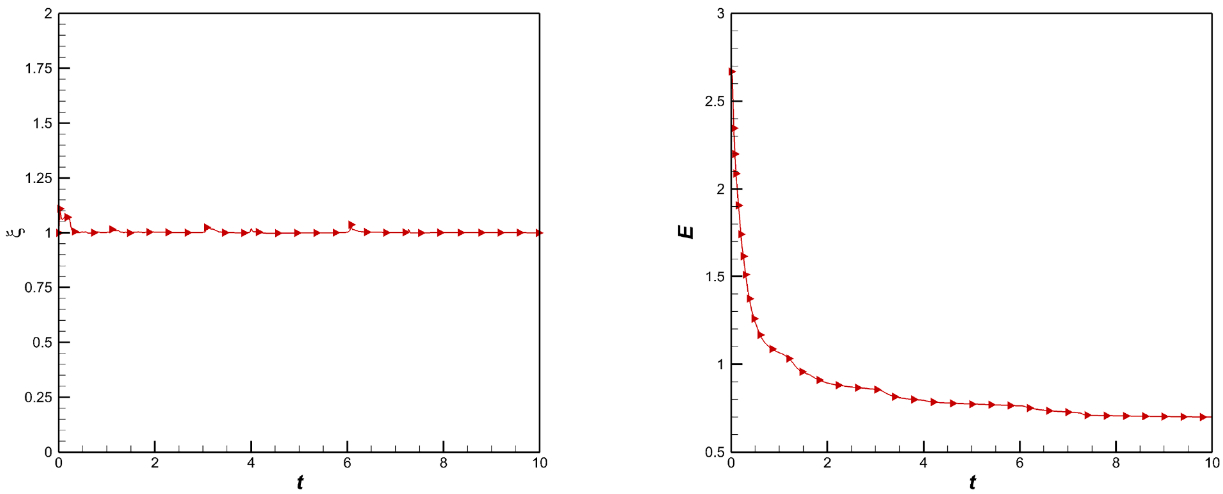

Fig. 8. Evolution of key quantities. Left: relaxation factor ξ, right: original energy E (Example 4).

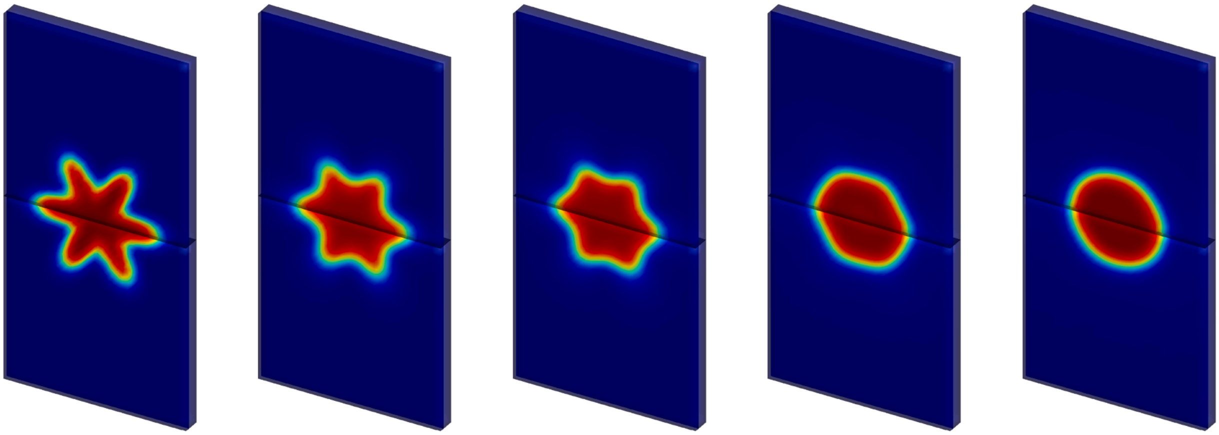

Fig. 9. Surface tension-driven droplet relaxation (n = 6, d = 3) at T = 0, 0.0006, 0.001, 0.002, 0.003.

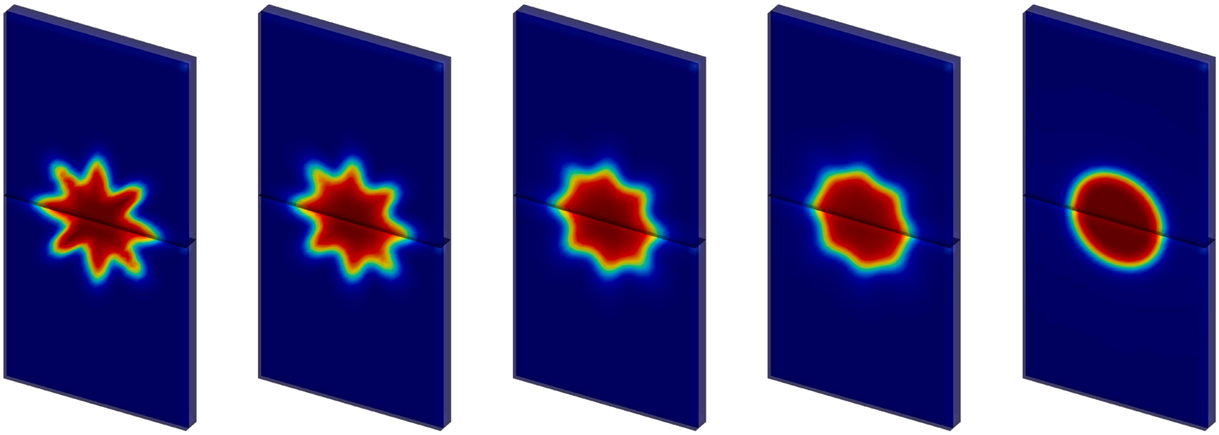

Fig. 10. Surface tension-driven droplet relaxation (n = 6, d = 3) at T = 0, 0.0001, 0.0003, 0.0005, 0.003.

As evidenced in Fig. 7, the phase field variable exhibits random spatial distribution throughout the domain at initial time. With time evolution, surface tension effects drive progressive phase separation, leading to the emergence of distinct domains characterized by sharp interfacial boundaries. The time evolution of the relaxation factor ξ, together with that of the original energy, is displayed in Fig. 8. The system ultimately evolves into stable, coarsened regions with minimized interfacial energy, in agreement with [55].

6.6. Example 5: Surface tension-driven droplet relaxation

This numerical example simulates the phase relaxation phenomenon. We generalize the problem to three dimensions, and define domain as $\Omega_c = (0, 0.1a) \times (0, a) \times (0, a)$, $\Omega_m = (0, 0.1a) \times (0, a) \times (a, 2a)$, $a = 0.35$. The initial phase field variable is given by

$$\phi^0 = \tanh\left(\frac{\min\{0.1 - x, 0.25a + 0.1a\cos(n\arctan\frac{z-a}{y-0.5a}) - \sqrt{(y-0.5a)^2 + (z-a)^2}\}}{\sqrt{2}\epsilon}\right).$$

We set $\Delta t = 1.0 \times 10^{-5}$, $T = 0.003$, $h = 1/64$, $M = 0.05$, $\mathbb{K} = 0.1\mathbb{J}$, with the other parameters the same as those in the above test. The results for $n = 6$ and $n = 8$ (where n denotes the number of petals in the initial shape) are presented in Figs. 9 and 10, respectively. As shown in these figures, the initial droplet in the central region progressively evolves into a circular shape under the action of surface tension over time. This evolution is consistent with the energy dissipation property of the Cahn–Hilliard–Navier–Stokes–Darcy model, which aligns with the physical characteristics of the model and corroborates the findings in [38,56,57]. The time evolution of the relaxation factor ξ, together with that of the original energy, is displayed in Fig. 11.

6.7. Example 6: Buoyancy-driven bubble rising

We investigate bubble dynamics in a two-phase flow driven by buoyancy force in this example. We add the buoyancy term $\mathbf{B}(\phi - \bar{\phi})$ at the right of (5.1) and (5.8), where $\mathbf{B} = (0, 5)^T$ and $\bar{\phi}$ represents the spatially averaged order parameter. The computational domain

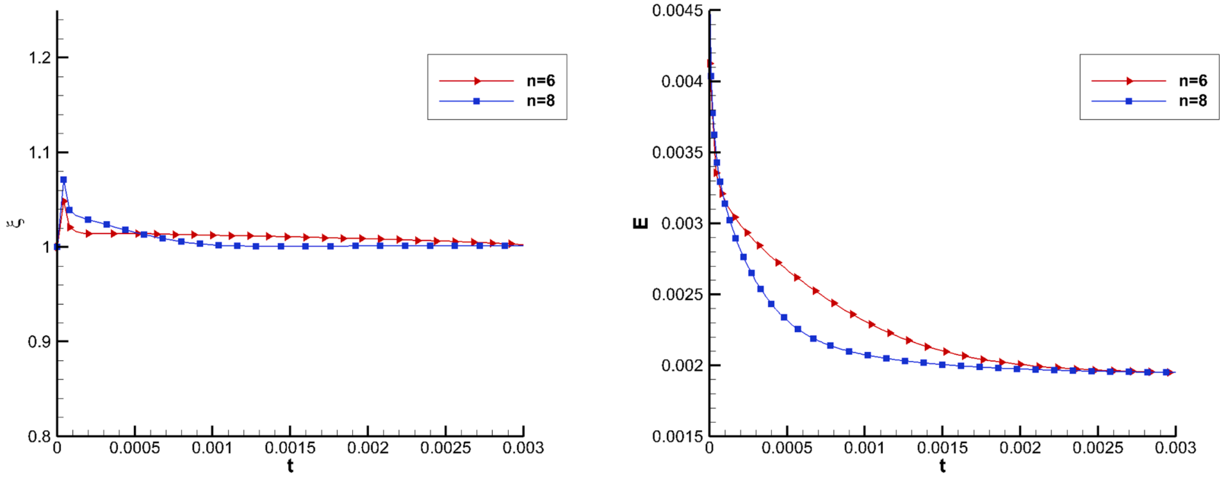

Fig. 11. Evolution of key quantities. Left: relaxation factor ξ, right: original energy E (Example 5).

and other parameters are consistent with Example 5. Initially, we set the phase variable as

$$\phi^0 = \tanh\left(\frac{R - \sqrt{(x - x_0)^2 + (y - y_0)^2}}{\sqrt{2}\epsilon}\right),$$

where $R = 0.3, x_0 = 0.5, y_0 = 0.5$. Fig. 12 illustrates the evolution of a bubble in the free-flow domain gradually rising toward the porous-media domain under buoyancy force, precisely capturing the moment when the bubble crosses the interface between the two domains.

Next, we set $\mathbf{B} = (0, 8)^T$, and consider that there are two initial bubbles in the free-flow domain. As shown in Figs. 13–14, the two bubbles rise by buoyancy and progressively merge while crossing the interface, which is consistent with [37,38]. And the evolution of ξ is presented in Fig. 15.

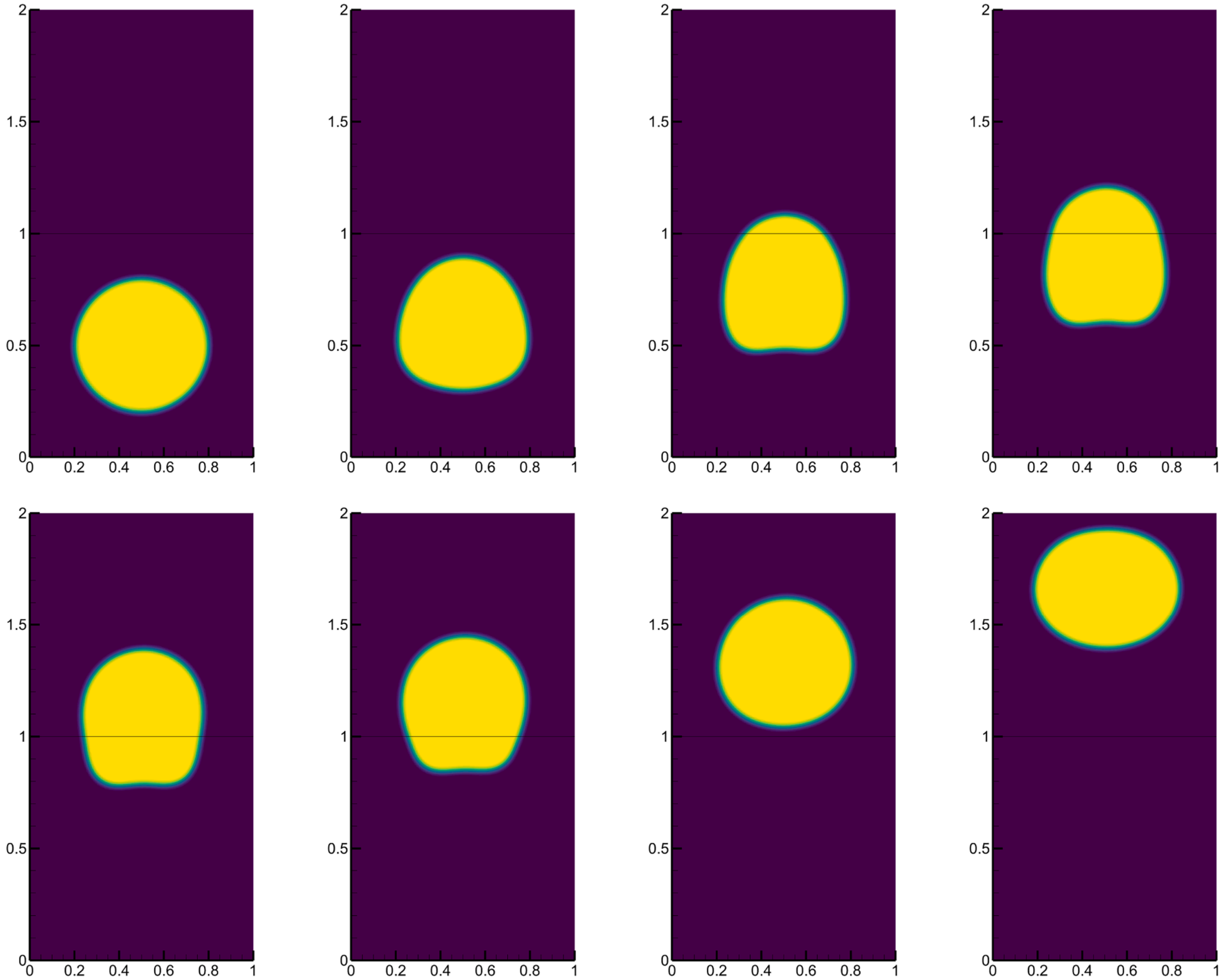

Fig. 12. Buoyancy-driven bubble rising at T = 0, 0.4, 1, 1.4, 2, 2.2, 2.8, 4.

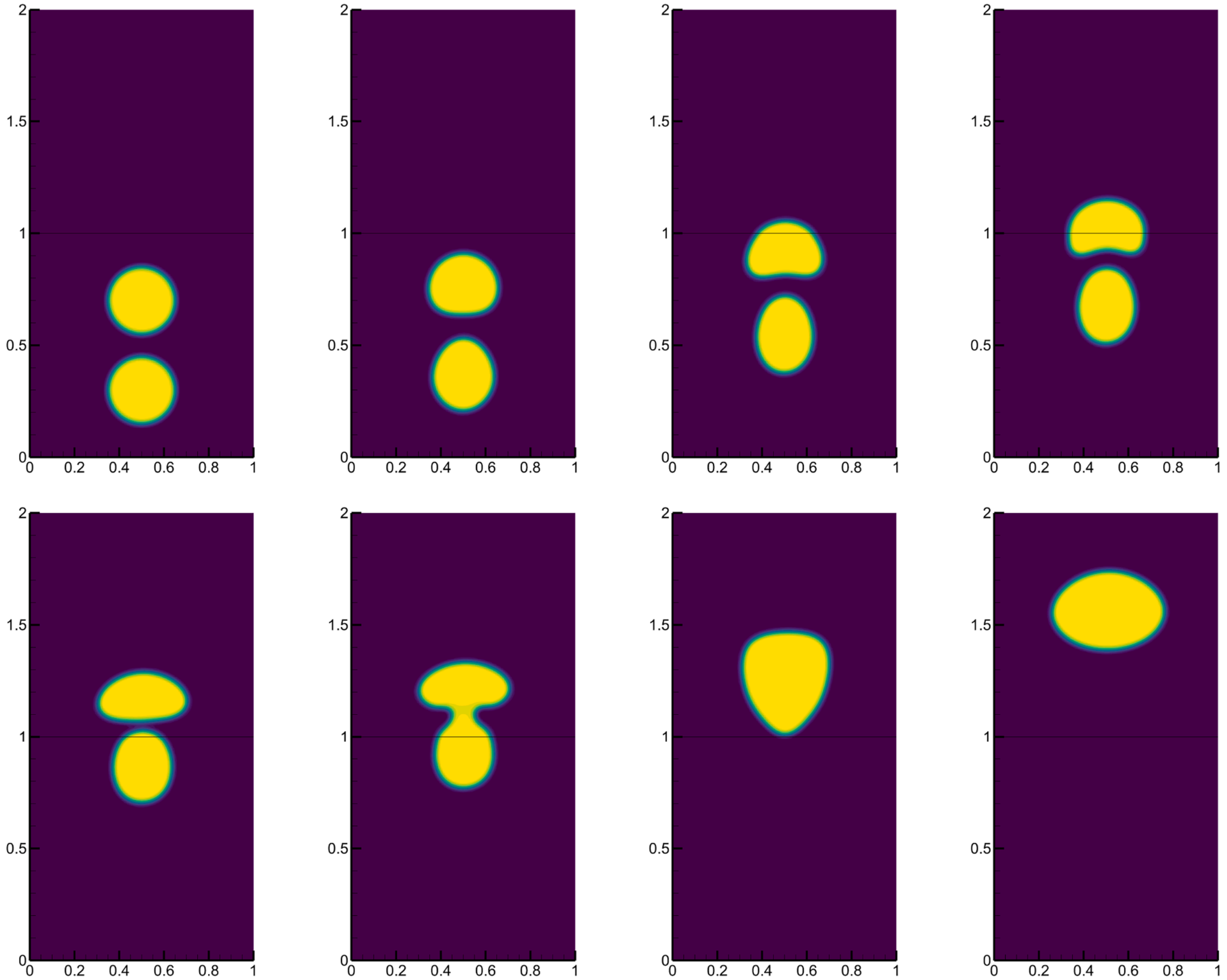

Fig. 13. Buoyancy-driven bubble rising at T = 0, 0.2, 0.5, 0.7, 1, 1.1, 1.4, 2.

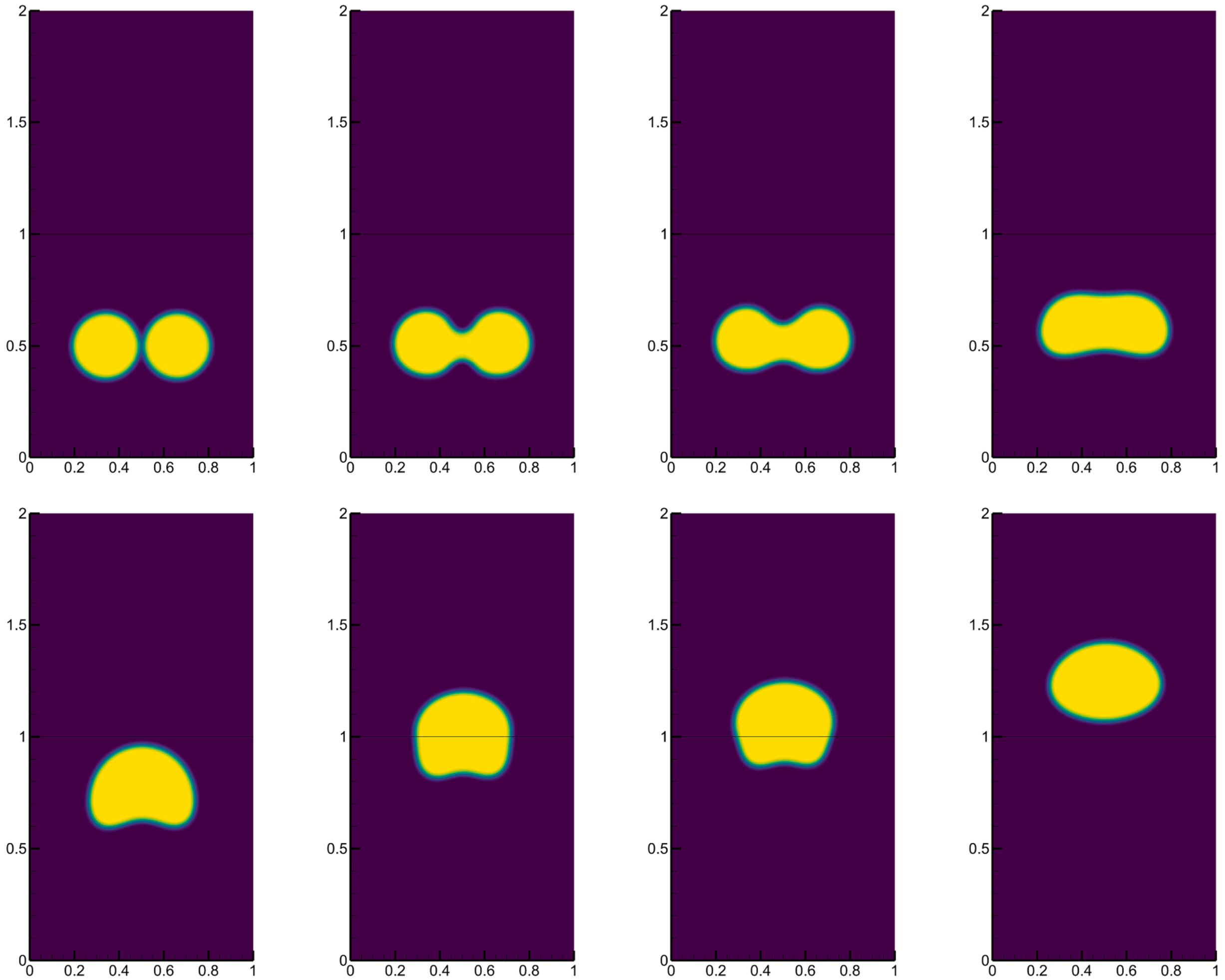

Fig. 14. Buoyancy-driven bubble rising at T = 0, 0.1, 0.2, 0.5, 1, 1.5, 1.6, 2.

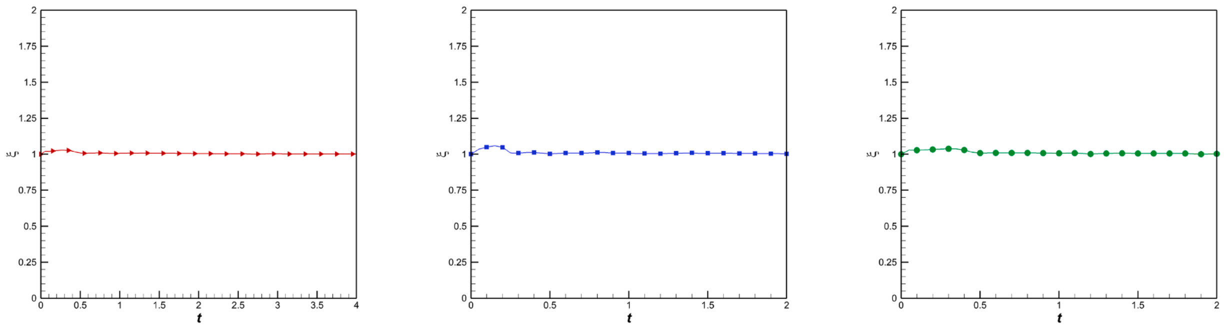

Fig. 15. The evolution of ξ over time in a buoyancy-driven bubble rise. Left: with one initial bubble, middle: with two initially vertically aligned bubbles, right: with two initially horizontally aligned bubbles (Example 6).

7. Conclusion

We developed in this paper novel linear and decoupled numerical schemes under a new relaxation mechanism for the Navier–Stokes–Darcy model and Cahn–Hilliard–Navier–Stokes–Darcy model. A key advantage of the proposed schemes is their computational efficiency, as they only require solving linear systems with constant coefficients at each time step. An essential property of these schemes is that they unconditionally dissipate the original energy. We rigorously established the unconditional stability of the proposed schemes, and as an example, derived optimal error estimates of the first-order scheme for the Navier–Stokes–Darcy model.

In numerical implementation, we adopted a finite element method with the EMAC formulation which can further preserve mass, momentum, and angular momentum at the discrete level. We presented several numerical experiments which validated the essential properties and robustness of the proposed schemes.

Data availability

No data was used for the research described in the article.

CRediT authorship contribution statement

Xiaoli Li: Writing – original draft, Methodology, Investigation, Funding acquisition, Formal analysis, Conceptualization; **Jie Shen:** Writing – review & editing, Methodology, Funding acquisition, Formal analysis, Conceptualization; **Xinhui Wang:** Writing – original draft, Validation, Methodology, Investigation, Formal analysis, Conceptualization.

Declaration of interests

The authors declare that they have no known competing financial interests or personal relationships that could have appeared to influence the work reported in this paper.

References

[1] A.A. Hill, B. Straughan, Poiseuille flow in a fluid overlying a porous medium, J. Fluid Mech. 603 (2008) 137–149.
[2] M. McCurdy, N. Moore, X. Wang, Convection in a coupled free flow-porous media system, SIAM J. Appl. Math. 79 (6) (2019) 2313–2339.
[3] M. Discacciati, Domain decomposition methods for the coupling of surface and groundwater flows, PhD thesis EPFL (2004).
[4] W.J. Layton, F. Schieweck, I. Yotov, Coupling fluid flow with porous media flow, SIAM J. Numer. Anal. 40 (2002) 2195–2218.
[5] N.S. Hanspal, A. Waghode, V. Nassehi, R.J. Wakeman, Numerical analysis of coupled stokes/darcy flows in industrial filtrations, Transp. Porous Media 64 (2006) 73–101.
[6] K.A. Mardal, X.-C. Tai, R. Winther, A robust finite element method for Darcy–Stokes flow, SIAM J. Numer. Anal. 40 (5) (2002) 1605–1631.
[7] Y. Cao, M. Gunzburger, F. Hua, X. Wang, Coupled Stokes–Darcy model with Beavers–Joseph interface boundary condition, Commun. Math. Sci. 8 (2010) (2010) 1–25.
[8] X. He, J. Li, Y. Lin, J. Ming, A domain decomposition method for the steady-State Navier–Stokes–Darcy model with Beavers–Joseph interface condition, SIAM J. Sci. Comput. 37 (5) (2015) S264–S290.
[9] L. Badea, M. Discacciati, A. Quarteroni, Numerical analysis of the Navier–Stokes/Darcy coupling, Numer. Math. 115 (2) (2010) 195–227.
[10] M. Cai, M. Mu, J. Xu, Numerical solution to a mixed Navier–Stokes/Darcy model by the two-grid approach, SIAM J. Numer. Anal. 47 (5) (2009) 3325–3338.
[11] P. Chidyagwai, B. Rivière, On the solution of the coupled Navier–Stokes and Darcy equations, Comput. Methods Appl. Mech. Eng. 198 (47–48) (2009) 3806–3820.
[12] Y. Cao, Y. Chu, X. He, M. Wei, Decoupling the stationary Navier–Stokes–Darcy system with the Beavers–Joseph–Saffman interface condition, Abstr. Appl. Anal. 2013 (2013) 1–10.
[13] V. Girault, B.M. Rivière, DG Approximation of coupled Navier–Stokes and Darcy equations by Beaver–Joseph–Saffman interface condition, SIAM J. Numer. Anal. 47 (2009) 2052–2089.
[14] M.-C. Shiue, K.C. Ong, M.-C. Lai, Convergence of the MAC scheme for the Stokes/Darcy coupling problem, J. Sci. Comput. 76 (2018) 1216–1251.
[15] A. Çesmelioglu, V. Girault, B.M. Rivière, Time-dependent coupling of Navier–Stokes and Darcy flows, Math. Model. Numer. Anal. 47 (2013) 539–554.
[16] C. Qiu, X. He, J. Li, Y. Lin, A domain decomposition method for the time-dependent Navier–Stokes–Darcy model with Beavers–Joseph interface condition and defective boundary condition, J. Comput. Phys. 411 (2020) 109400.
[17] W. Chen, M. Gunzburger, D. Sun, X. Wang, Efficient and long-time accurate second-order methods for the Stokes–Darcy system, SIAM J. Numer. Anal. 51 (5) (2013) 2563–2584.
[18] M. McCurdy, N.J. Moore, X. Wang, Predicting convection configurations in coupled fluid-porous systems, J. Fluid Mech. 953 (2022) A23.
[19] H. Rui, J. Zhang, A stabilized mixed finite element method for coupled Stokes and Darcy flows with transport, Comput. Methods Appl. Mech. Eng. 315 (2017) 169–189.
[20] W. Chen, D. Han, X. Wang, Y. Zhang, Uniquely solvable and energy stable decoupled numerical schemes for the Cahn–Hilliard–Navier–Stokes–Darcy–Boussinesq system, J. Sci. Comput. 85 (2020) 45.
[21] S. Caucao, R. Oyarzúa, S. Villa-Fuentes, A priori and a posteriori error analyses of a fully-mixed finite element method for the coupled Navier–Stokes/Darcy problem, Comput. Methods Appl. Mech. Eng. 450 (2026) 118598.
[22] Y. Hong, W. Zhang, L. Zhao, H. Zheng, Coupling finite element and multiscale finite element methods for the non-stationary Stokes-Darcy model, J. Comput. Phys. 530 (2025) 113899.
[23] L. Lin, Z. Yang, S. Dong, Numerical approximation of incompressible Navier–Stokes equations based on an auxiliary energy variable, J. Comput. Phys. 388 (2018) 1–22.
[24] X. Li, J. Shen, Error analysis of the SAV–MAC scheme for the Navier–Stokes equations, SIAM J. Numer. Anal. 58 (5) (2020) 2465–2491.
[25] J. Shen, J. Xu, J. Yang, The scalar auxiliary variable (SAV) approach for gradient flows, J. Comput. Phys. 353 (2018) 407–416.
[26] J. Shen, J. Xu, Convergence and error analysis for the scalar auxiliary variable (SAV) schemes to gradient flows, SIAM J. Numer. Anal. 56 (2018) 2895–2912.
[27] X. Li, J. Shen, Z. Liu, New SAV–pressure correction methods for the Navier–Stokes equations: stability and error analysis, Math. Comput. 91 (2022) 141–167.
[28] X. Li, J. Shen, On fully decoupled MSAV schemes for the Cahn–Hilliard–Navier–Stokes model of two-phase incompressible flows, Math. Models Methods Appl. Sci. 32 (03) (2022) 457–495.
[29] N. Jiang, H. Yang, SAV decoupled ensemble algorithms for fast computation of Stokes–Darcy flow ensembles, Comput. Methods Appl. Mech. Eng. 387 (2021) 114150.
[30] N. Jiang, H. Yang, Fast and accurate artificial compressibility ensemble algorithms for computing parameterized Stokes–Darcy flow ensembles, J. Sci. Comput. 94 (1) (2023) 17.
[31] X. Wang, X. Guo, X. Li, A class of new linear, efficient and high-order implicit–explicit methods for the unsteady Navier–Stokes–Darcy model based on nonlinear lions interface condition, J. Sci. Comput. 101 (2) (2024) 40.
[32] Q. Cheng, C. Liu, J. Shen, A new Lagrange multiplier approach for gradient flows, Comput. Methods Appl. Mech. Eng. 367 (2020) 113070.
[33] Y. Gao, X. He, L. Mei, X. Yang, Decoupled, linear, and energy stable finite element method for the Cahn–Hilliard–Navier–Stokes–Darcy phase field model, SIAM J. Sci. Comput. 40 (1) (2018) B110–B137.
[34] Y. Wu, Y. Gao, X. He, Y. Lin, Optimal error estimates for a semi-discrete finite element scheme of Cahn–Hilliard–Navier–Stokes–Darcy model, Commun. Nonlinear Sci. Numer. Simul. 152 (2025) 109257.

[35] J. Chen, S. Sun, X.-P. Wang, A numerical method for a model of two-phase flow in a coupled free flow and porous media system, J. Comput. Phys. 268 (2014) 1–16.
[36] D. Han, X. He, Q. Wang, Y. Wu, Existence and weak–strong uniqueness of solutions to the Cahn–Hilliard–Navier–Stokes–Darcy system in superposed free flow and porous media, Nonlinear Anal. 211 (2021) 112411.
[37] W. Chen, D. Han, X. Wang, Uniquely solvable and energy stable decoupled numerical schemes for the Cahn–Hilliard–Stokes–Darcy system for two-phase flows in karstic geometry, Numer. Math. 137 (1) (2017) 229–255.
[38] Y. Gao, X. He, T. Lin, Y. Lin, Fully decoupled energy-stable numerical schemes for two-phase coupled porous media and free flow with different densities and viscosities, ESAIM: Math. Model. Numer. Anal. 57 (3) (2023) 1323–1354.
[39] R. Temam, Navier–Stokes Equations: Theory and Numerical Analysis, North-Holland Pub. Co., 1977.
[40] V. Girault, P.-A. Raviart, Finite Element Methods for Navier–Stokes Equations: Theory and Algorithms, Springer Science & Business Media, 2012.
[41] J. Bear, Hydraulics of Groundwater, Courier Corporation, 2012.
[42] G.S. Beavers, D.D. Joseph, Boundary conditions at a naturally permeable wall, J. Fluid Mech. 30 (1) (1967) 197–207.
[43] P.G. Saffman, On the boundary condition at the surface of a porous medium, Stud. Appl. Math. 50 (2) (1971) 93–101.
[44] J. Shen, On error estimates of projection methods for Navier–Stokes equations: first-order schemes, SIAM J. Numer. Anal. 29 (1992) 57–77.
[45] J.M. Connors, J.S. Howell, A fluid–fluid interaction method using decoupled subproblems and differing time steps, Numer. Methods Partial Differ. Equations 28 (2012) 1283–1308.
[46] H. Abels, Diffuse Interface Models for Two-Phase Flows of Viscous Incompressible Fluids, Ph.D. thesis, 2008.
[47] M.E. Gurtin, D. Polignone, J. Vinals, Two-phase binary fluids and immiscible fluids described by an order parameter, Math. Models Methods Appl. Sci. 6 (06) (1996) 815–831.
[48] E. Weinan, P. Palffy-Muhoray, Phase separation in incompressible systems, Phys. Rev. E 55 (4) (1997) R3844.
[49] X. Feng, S. Wise, Analysis of a Darcy–Cahn–Hilliard diffuse interface model for the Hele-Shaw flow and its fully discrete finite element approximation, SIAM J. Numer. Anal. 50 (3) (2012) 1320–1343.
[50] F. Hecht, New development in freeFem++, J. Numer. Math. 20 (3–4) (2012) 251–266.
[51] M.A. Olshanskii, L.G. Rebholz, Longer time accuracy for incompressible Navier–Stokes simulations with the EMAC formulation, Comput. Methods Appl. Mech. Eng. 372 (2020) 113369.
[52] S. Charnyi, T. Heister, M.A. Olshanskii, L.G. Rebholz, On conservation laws of Navier–Stokes Galerkin discretizations, J. Comput. Phys. 337 (2017) 289–308.
[53] Y. Zhang, L. Mei, R. Li, A hybrid high-order method for a coupled Stokes–Darcy problem on general meshes, J. Comput. Phys. 403 (2020) 109064.
[54] R. Li, Y. Gao, J. Li, Z. Chen, A weak Galerkin finite element method for a coupled Stokes–Darcy problem on general meshes, J. Comput. Appl. Math. 334 (2018) 111–127.
[55] X. Li, Z. Liu, J. Shen, N. Zheng, On a class of higher-order fully decoupled schemes for the Cahn–Hilliard–Navier–Stokes system, J. Sci. Comput. 103 (1) (2025) 1–28.
[56] Y. Gao, D. Han, Second-order decoupled linear energy-law preserving gPAV numerical schemes for two-phase flows in superposed free flow and porous media, J. Sci. Comput. 100 (2) (2024) 36.
[57] Y. Gao, R. Li, X. He, Y. Lin, A fully decoupled numerical method for Cahn–Hilliard–Navier–Stokes–Darcy equations based on auxiliary variable approaches, J. Comput. Appl. Math. 436 (2024) 115363.